A dissertation proposal

Working title: Waste-heat-driven cooling systems for hot, dry climates

Submitted by: Nicholas W Fette

Degree program: Doctor of philosophy in mechanical engineering

Committee members:

Patrick E Phelan (co-chair)
Harvey J Bryan (co-chair)
Steven Trimble
Ellen B Stechel
Liping Wang

Administrative unit:

Mechanical Engineering
School of Engineering for Matter, Transport, and Energy
Arizona State University

Contents

List of figures iv
List of Tables vi
1 Introduction 1
1.1 Overview 1
1.2 Status and publication schedule 2
1.3 Application focus 2
1.4 Nomenclature 4
2 Waste-heat-driven cooling system selection 5
2.1 Introduction 5
2.1.1 Purpose 5
2.1.2 Technologies to be compared and status of work 6
2.1.3 Chapter outline 6
2.2 Methods and assumptions 7
2.2.1 System level design 7
2.2.2 Background for heat exchanger plots 8
2.2.3 Heat transfer models 10
2.2.4 Constraints, objective function, and optimization technique 12
2.3 Water ejector cycle 12
2.3.1 Ejector cycle methods and assumptions 12
2.3.2 Ejector system modeling results 15
2.4 Single-effect lithium-bromide absorption cycle 19
2.4.1 Absorption cycle methods and assumptions 19
2.4.2 Absorption cycle modeling results 21
2.5 Single-effect ammonia-water cycle 22
2.5.1 Pumped flow rate parameter study 23
2.5.2 Optimization results 25
2.6 Cooling technology comparison 25
2.7 Conclusions and future work 26
3 Heat rejection system selection and water usage control 27
3.1 Introduction and purpose 27

3.2 Heat rejection system models 27
3.2.1 Heat rejection technologies to be included 27
3.2.2 Performance models and metrics 28
3.2.3 Indirect evaporative cooling tower model 29
3.3 Inlet cooling comparison 32
3.4 Conservative controls for heat rejection 33
3.5 Summary and next steps 36
4 Cooling in high ambient temperatures 37
4.1 Introduction 37
4.1.1 Some data about ambient temperatures and rating conditions 37
4.2 Future work: matching heat input demand to heat source 38
4.2.1 Multiple chillers 38
4.2.2 Custom absorption chiller design 40
4.2.3 Ejector cycles with mixtures 41
4.2.4 Fluid selection for trans-critical ejector cycle 42
4.3 Future work: modified cycles at high ambient temperatures 42
4.4 Miscellaneous methods 43
4.5 Summary and next steps 44
5 Summary 45
6 Acknowledgements 46
7 Works Cited 47

List of figures

Figure 1. Hypothetical example of a heliostat array and tower for concentrating solar power generation. 3
Figure 2. System level flow schematic. [TODO: 31->32 should be counterflowing 27->21. Fix this, or find diagram from AORA slides (I mean slides I made for AORA).] Worker model provided by [8] for non-commercial use only. 7
Figure 3. Sequential heat exchange example and plot concept. 8
Figure 4. Hypothetical example of a grand composite curve for process heating and cooling demand. 9
Figure 5. Flow schematic of non-contacting heat exchanger. 10
Figure 6. Ejector cycle process. The components on the left form a power cycle that acts as the compressor for the refrigeration cycle, with shared condenser. 13
Figure 7. Schematic for heat exchangers in ejector cycle. 13
Figure 8. Ejector cycle typical process in state-space representation of ejector cycle 15
Figure 9. Inverse trends of COP and generator heat input for different levels of ambient temperature (indicated for each curve). The x-axis is the generator saturation temperature. 16
Figure 10. Optimum design of generator temperature. 17
Figure 11. Dependence on ambient temperature of optimal allocation of heat exchanger area to maximize cooling capacity, with total UA of 16.61 kW/K. 18
Figure 12. Area-constrained optimization of cooling capacity by varying allocation of heat exchange surface area. Solid curves show maximum cooling capacity and dashed curves show optimal generator saturation temperature. The variation with ambient temperature, for various levels of total UA, is shown. 19
Figure 13. System schematic with LiBr single effect chiller. Based on original diagram from [10]. [TODO: update state point indices.] 20
Figure 14. Liquid and vapor streams in generator. States 4 and 8 are in equilibrium, and external heat exchange occurs with liquid stream. 20
Figure 15. The concentration in the two streams varies with flow rate. When the flow rate is very high, the concentrations are equal, setting an upper limit for flow rate in the plots for this section. 21
Figure 16. Running the solver updates this depiction of the internal state points as a check for crystallization against the solubility limit given in [10]. This was used to establish the crystallization limits in Figure 17. 22
Figure 17. For each shown value of chiller designed with the catalog method and optimum pump rate, the variation of cooling capacity with ambient temperature is shown. For high ambient temperatures, the expanded strong solution crosses the crystallization boundary. (This could be mitigated by adding heat to that stream, requiring additional heat rejection and decreasing performance.) 22
Figure 18. Cycle diagram of a simple single-effect ammonia-water absorption cycle. The box on right indicates the heat recovery and transport loop. 23
Figure 19. The concentration in the solution streams varies with pumped flow rate. 24
Figure 20. Stream temperatures in single effect ammonia-water parametric study. 24

Figure 21. Heat flows for the single parameter study of a simple single-effect absorption cycle with ammonia-water. 25
Figure 22. Some optimization results for ammonia-water absorption cycle model. 25
Figure 23. Cooling capacity comparison between technologies at several levels of cost proxy. 26
Figure 24. Cooling tower performance: for 50% effectiveness, contours of cooled water outlet temperature and water consumption rate over psychrometric state space for direct (left) and indirect cooling towers (right). 29
Figure 25. A heat transfer diagram for a direct evaporative cooling tower from ASHRAE [29]. 30
Figure 26. Multiple cells allow more accurate model of the direct contact heat exchange and evaporation process. Image taken from [35]. 31
Figure 27. Example multicell calculation of an evaporative process for humidification and heating from literature [33]. 32
Figure 28. Inlet cooling capacity requirement per turbine. 33
Figure 29. Probability distributions of ambient conditions calculated from TMY3 data for Phoenix [36]. 34
Figure 30. Cumulative probability distributions of some effective temperatures for dry bulb and dew point, including direct evaporative cooler (DEC) and indirect evaporative cooler (IDEC), again calculated from TMY3 data for Phoenix [36]. 34
Figure 31. Possible water consumption allocation as a function of ambient condition based on probability, shown as contours of water consumption per unit of heat rejected (kg/kJ) over the psychrometric state space. 35
Figure 32. Possible probability distribution for cooled water outlet temperature resulting from control algorithm and simulation with historical data. 35
Figure 33. Some data about ambient temperatures, from [18]. 37
Figure 34. Multiple chillers drawing heat from heat source in series: conceptual schematic (left, not actual temperatures) and rescaled heat exchange diagram (right). Box areas show exergy supplied to the high effect chiller (red) and low effect (blue). 39
Figure 35. Multiple chillers: naïve model trends for optimal configurations. 40
Figure 36. Multiple chillers: optimal temperatures for each case from one through five chillers. 40
Figure 37. Conceptual schematic (left) for a custom chiller design intended to match the heat source profile. Increasing the number of levels could allow the grand composite curve for heat input to approach an ideal case (right). [TODO: re-draw figure on right] 41
Figure 38. Some state points from numerical model of ejector cycle with a mixture of 40% by mass ethanol in water. 42
Figure 39. A cycle modified to recover energy from refrigerant expansion, from [46]. 43

List of Tables

Table 1. Ejector cycle internal state points. 13
Table 2. Ejector pump model coefficients and values for water as a working fluid. 14
Table 3. State point assumptions for LiBr single-effect chiller model. 21
Table 4. Internal state points for ammonia-water absorption cycle 22
Table 5. Applicable test standards for condenser external temperatures 38

1 Introduction

1.1 Overview

Waste-heat-driven cooling including turbine inlet cooling is feasible using off-the-shelf technology, up to a certain threshold of ambient temperature. However, detailed system modeling is needed to optimize the cooling capacity subject to constraints on cost and water usage. The purpose of this dissertation is to illustrate techniques for optimal design of waste-heat-driven cooling in light of these constraints, with application to a novel thermal plant system. The work is divided into the three following chapters: chiller selection, water usage optimization, and chiller design for high ambient temperature.

In the work on chiller selection, we take the exhaust stream from a Brayton cycle engine and compare the cooling output from different heat-driven cooling technologies, showing which system provides the greatest cooling capacity, and how the chiller and heat transport equipment should be configured optimally for no water consumption. This work can be applied to the AORA Solar Tulip, which has previously utilized wet spray inlet cooling. Therefore the results help answer the important question: what is the potential to reduce water consumption without reducing power output and to provide an additional energy service to the customer? This work is on-going with significant findings reported.

In the next chapter, we outline future work to optimize the cooling system when a certain amount of annual water consumption is allowed, and answer the questions: what should be the system level design, component level design, and controls for the allocation of cooling water throughout the year? At the system level, we perform a technology comparison for relevant performance metrics as functions of ambient conditions. For chiller heat rejection we consider dry cooling, direct evaporative cooling, hybrid wet-dry cooling, indirect evaporative cooling, and ground source heat rejection. For inlet cooling we compare conventional spray inlet cooling to chiller-supplied cooling. At the component level, we draw from an on-going work for design, analysis, and construction of an indirect evaporative cooling tower to identify the parameters that may be optimized in the context of multiple objectives for water conservation and cooling system performance and to determine sizing and cost information where published data are insufficient, since the technology remains relatively rare in the market. The controls may be based on real-time ambient conditions and demand and any available information about the annual average distribution of ambient conditions. Given that information, the control algorithm should also be able to demonstrate in simulation the ability to satisfy the water constraint at a given confidence interval.

In the final chapter we outline focus on the effect of high ambient temperatures and analyze the changes in standard cooling cycle performance, then consider several options for cooling cycles that operate robustly under those conditions. In this we also include ejector cooling cycles and hybrid combinations such as ejector-assisted absorption cooling. Additionally, we consider an absorption cycle design approach based on matching the heat vs temperature profile of a Brayton turbine.

1.2 Status and publication schedule

Topic	Publication submission or work date goals
Technology performance comparison	October 2015
• Define problem • LiBr model • LiBr plus heat exchange model • LiBr optimal curves • Ejector cycle model • Ejector cycle plus heat exchange model • Ejector cycle optimal curves • Ammonia-water model • Ammonia-water plus heat exchange model • Ammonia-water optimal curves	• 2009 (Bombarda et al.) • 1996 (Herold et al.) • 1996 (Herold et al.) • Spring-Summer 2015 • 1985 (Tyagi et al.) • Spring 2015 • Summer 2015 • 1996 (Herold et al.) • Aug.-Sept. 2015 • Sept.-Oct. 2015
Heat rejection selection	January 2016
• Numerical model and experiment of cooling tower • Reading to define problem • Other work TBD	• Sept. 2013 to June 2014 • June-October 2015 • Nov.-Dec. 2015
High ambient temperatures	May 2016
• Existence of optimal configuration for multiple chillers • Analytical result for simplified configuration of multiple ideal chillers • Ejector cycle with mixture • Reading to define problem	• August 2014 • August 2015 • Spring 2015 • Jan 2016

1.3 Application focus

The AORA Tulip depicted in Figure 1. Hypothetical example of a heliostat array and tower for concentrating solar power generation.Figure 1 is unique among solar power towers for its small scale and technology. The 100 kW_e nominal rating allows for the use of a packaged microturbine and other commercial off-the-shelf (COTS) technology, and also reduces the scale requirement for a purchaser to enter the thermal concentrating solar power (CSP) market from the multi-megawatt utility scale [1]. The open-cycle Brayton turbine allows for zero water consumption, as no heat rejection occurs except in the direct contact of the exhaust stream returned to the environment. Additionally, gas hybridization means that the system can provide renewable and firm power without thermal storage at the high temperatures required for the Brayton cycle. Potential fuel stocks include biofuels from sustainable sources such as waste bio-mass or waste-fed algae and solar fuels with low net carbon footprint.

Based on the potential target markets for the system, several factors distinguish the design criteria of a cooling system driven by the AORA Tulip from cooling system designs for utility and commercial scale combined cooling, heat, and power (CCHP) plants outlined in [2]. First, the turbine exit temperature of the exhaust stream is sufficiently low (270 °C) that the tradeoff between different cooling technologies operating at different driving temperatures becomes non-trivial. Second, the small capacity suggests a preference for commercialized technology in order to benefit from scale production, but the trade-off

between performance and cost of custom design must be analyzed. Third, there is a preference for low to no water consumption. Evaporative cooling is typically assumed to limit the chiller heat rejection temperatures, and therefore a cooling system must be suitable for operating in high ambient temperatures. Separately from the present work, utilization of the Tulip waste heat for desalination and water treatment is also being addressed.

In this work, the microturbine in the AORA Tulip will be used to specify the model for the waste heat source, and design and results for cooling capacity are reported on a per-Tulip basis. The exhaust flow rate and temperature are described in the manufacturer's detailed specification [3]. A systematic and rigorous study on the potential of heat recovery for cooling using this system has not been found in the literature, and so is presented here.

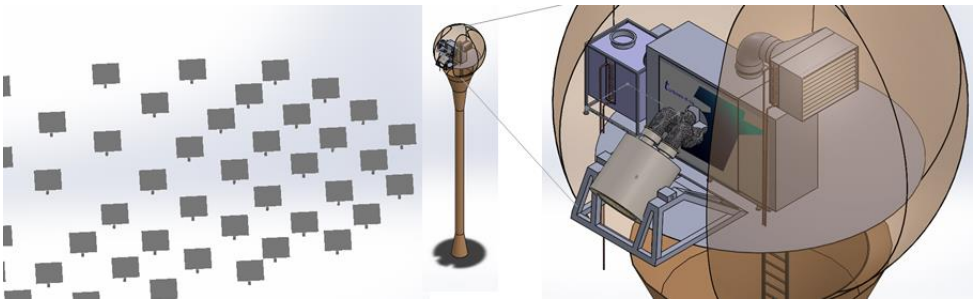

Figure 1. Hypothetical example of a heliostat array and tower for concentrating solar power generation.

1.4 Nomenclature

T	Temperature (°C or K)
ΔT	Temperature difference (K)
T_0	Reference temperature (eg. ambient) (K)
$\dot{m}$	Mass flow rate (kg/s)
$\dot{Q}$	Heat flow rate (kW)
h	Mass-specific enthalpy (kJ/kg)
U	Overall heat transfer coefficient (kW/m^2-K)
A	Area (m^2)
x	Vapor quality (kg/kg)
z	Mixture mass concentration (kg/kg)
c_p	Mass-specific heat at constant pressure (kJ/kg-K)
h_{fg}	Mass-specific latent heat of vaporization (kJ/kg)
R	Temperature difference ratio (K/K)
S	Stream heat capacity ratio ([kW/K]/[kW/K])
KE	Mass-specific kinetic energy (kJ/kg)
η_{nozzle}	Nozzle isentropic efficiency ([kJ/kg]/[kJ/kg])
$\eta_{entrainment}$	Entrainment efficiency
$\eta_{diffuser}$	Diffuser efficiency
λ	Entrainment ratio (kg/kg)
COP	Thermal coefficient of performance (kW/kW)
DEC	Direct evaporative cooler
IDEC	Indirect evaporative cooler
DB	Dry bulb temperature (°C)
WB	Wet bulb temperature (°C)

2 Waste-heat-driven cooling system selection

2.1 Introduction

This is a slightly abridged and modified version of the Heat driven cooling system selection report prepared for AORA by the author.

2.1.1 Purpose

Waste-heat-driven cooling has been applied to increase the net utility of thermal power plants, yielding CCHP systems [4]. A common heat-driven cooling technology for these applications is absorption cycle cooling, using lithium-bromide absorbent with water refrigerant for cooling temperatures above 5 °C or water as an absorbent with ammonia as refrigerant for lower temperatures and a larger range of cooling capacities. Other heat-driven cooling technologies have also been developed and marketed and are compared in [5]. The system designer tasked with selecting the cooling technology to use must have sufficient data about each option to make a comparison. Particularly, this work focuses on the case where the waste heat comes from an open cycle plant, such as a Brayton cycle gas- or solar-fired turbine, in which case there is a tradeoff regarding the set-point for the cooling cycle's internal boiler pressure. Increasing the boiler pressure set-point increases the saturation temperature, and in turn decreases the quantity of heat recovered from the heat source. Another trade-off is the allocation of cost among the heat transfer components, for which heat exchange area is a useful proxy. From a whole system perspective, the performance is a function of not only the chiller package, but also the heat recovery heat exchanger, and indeed the turbine set-points. Furthermore, the chiller will contain internal controls for pumped flows and expansion valves, which should be controlled with an understanding of the heat source trade-off. Therefore, cooling system optimization requires a whole-system thermodynamic/heat transfer model and a chiller design that may not coincide with the design choices in an off-the-shelf model.

As much as possible, chiller manufacturers' data should be used directly. Unfortunately, many COTS cooling systems are not sufficiently documented to determine performance over a wide range of conditions. For example, one absorption chiller manufacturer provides cooling capacity and hot water consumption at nominal rating conditions, and single parameter curves for de-rating with respect to temperatures of chilled water, heat rejection or cooling water, and part load (cooling capacity) [6]. However, one should not assume that performance can be determined by multiplying the de-rating factors when two or more of these parameters are adjusted away from nominal.

Using whole-system steady-state modelling, this chapter addresses the question of which technology offers the best value by first asking: for each cooling technology, what are the optimal chiller design and performance as functions of heat rejection temperature and system price cap? Cooling technology selection can then be based on requirements for cooling capacity, cost, and other factors such as reliability and safety. Furthermore, the optimal designs are compared to baseline chillers optimized for nominal rating conditions, to demonstrate the relevance of the method, and to provide data for making the decision whether a COTS chiller should be employed due to cost barriers for custom chiller fabrication, depending on the production scale.

A similar approach for comparing low grade heat recovery systems was published by Bombarda et al. [7]. In that work, the goal was power generation from a Diesel cycle exhaust stream. The approach was to identify parameters for optimal system design (mainly mixture concentrations and flow rates), then compare power generated by different cycles as functions of log mean temperature difference in the heat recovery heat exchanger, which is analogous to a comparison on an equal installed cost basis. Particularly, the Kalina cycle was suggested based on the potential of employing a non-azeotropic working fluid (which typically exhibits temperature glide in the boiler) to reduce the irreversibility of heat transfer from the waste heat source to the working fluid.

Other previous works have also looked at some aspects of the comparison, such as relations between (generator) heat input temperature and COP as in Sirwan et al. [8], with simpler assumptions.

2.1.2 Technologies to be compared and status of work

System models have been implemented for a number of technologies which received the most attention in literature on existing equipment and installations. Single-effect lithium bromide absorption and water-based single-stage ejector cycles, as well as a simple, idealized chiller model using a fraction of Carnot efficiency instead of a physical cycle. A model of an ethanol-water mixture in a single-stage ejector cycle was created, but was found to offer poor performance, and was not integrated into the system model. Existing chiller models have also been obtained for double- and triple-effect LiBr absorption, as well as ammonia-water absorption cycles. As ongoing work following the schedule in section 1.2, these and an adsorption chiller model will be added to the system optimization framework. A simple turbine model was also developed, which as a separate work will be adapted for a decision-system platform and extend the boundary of the system to include the effect of ambient temperature on turbine efficiency.

The bulk of the modeling here was performed using the paid academic version of F-chart Engineering's software package called Engineering Equation Solver (EES), a numerical solver with built-in thermodynamic property functions. Additional work was begun to enable the modeling in other languages for future studies; particularly, the properties for mixtures of ammonia-water and lithium bromide are not easily available in existing open software platforms (although ammonia-water mixtures are provided at relatively low cost in the NIST REFPROP database). A review of alternative modeling platforms was begun, and is suggested as a starting point for future work on turning the methods presented here into a useful software tool.

2.1.3 Chapter outline

The system level model is established first along with design choices, heat exchange modeling methods, and system optimization methods. Next are described the ejector cycle model and the results of its integration into the system model. In parallel structure, the single-effect LiBr absorption model and its results follow. The final section discusses the comparison of systems. Finally, conclusions and future work are presented.

2.2 Methods and assumptions

2.2.1 System level design

Figure 2 shows the scope of analysis and state points in the flow streams external to the chiller. The numbering was selected to simplify plotting of the cycle and heat transfer diagrams within the analysis software package. There are four streams, and the following paragraphs describe the heat exchanging components. In addition to the endpoints for the heat exchangers, some other points were added corresponding to the chiller internal saturation points, useful for labeling the pinch points as will be discussed in the next section.

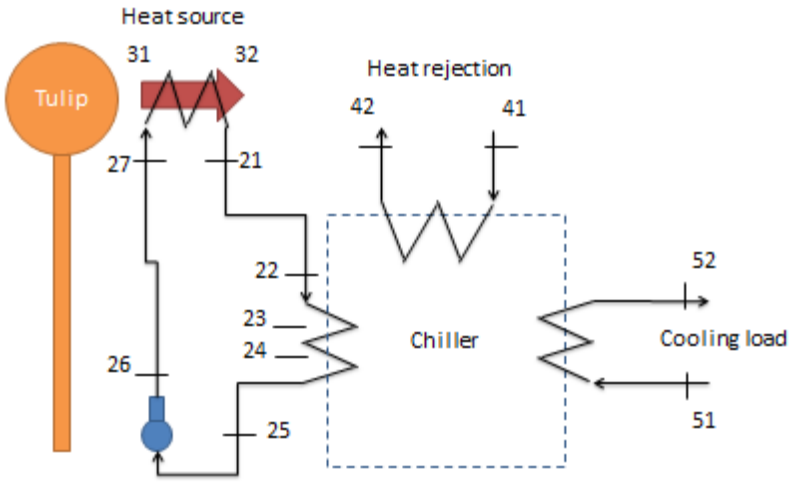

Figure 2. System level flow schematic. [TODO: 31->32 should be counterflowing 27->21. Fix this, or find diagram from AORA slides (I mean slides I made for AORA).] Worker model provided by [9] for non-commercial use only.

The exhaust stream (points 51, 52) enters the system after exiting the turbine recuperator, and is specified at this point by the turbine manual. A counterflow heat exchanger, called the heat recovery heat exchanger (HRHX), is assumed as a design choice to indirectly transfer heat to a heat transport fluid (HTF) stream (points 21 to 27). In the analysis we neglect head loss due to dissipation and pressure changes from buoyancy, treating the HTF as saturated liquid water at each point. We also model the heat loss to ambient as a fixed heat flow. These assumptions are justified by the limited intent to analyze the cooling cycle; a refined model of the transport system has also been created to determine the design pressures, pumping work, and heat losses depending on pipe size, length, and ambient temperature, which will be used specifically for the transport loop design following selection of the chiller and its maximum driving temperature. A latent heat transport loop will be considered as a design option but may not preferred due to the adverse effect of buoyancy on transporting heat downward against gravity. For example, sending saturated steam down a 30 m drop would produce a large amount of condensate, and superheating increases the required pipe size and subsequent ambient heat loss. Aside from water, other sensible HTFs may be used, such as Dowtherm products, to reduce pipe pressures.

The other end of the heat transport loop passes through another counterflow heat exchanger, referred to as the generator component inside the chiller, which can be considered as a boiler for the moment. The chiller's evaporator takes in heat from a chilled water stream (points 31 and 32) via a counterflow heat exchanger. The chiller rejects heat through one or more counterflow heat exchangers to a sensible heat rejection stream, nominally entering at ambient temperature (point 41). This loop is also modeled as saturated liquid water, which is justified by the fact that a larger mass flow rate of air could produce the same characteristic stream heat capacity, or the heat exchanger model could capture the total thermal impedances of both an internal condenser-to-water heat exchanger and external water-to-air exchanger.

2.2.2 Background for heat exchanger plots

It is common practice to visualize (with no equations required) the heat transfer between two counterflowing, non-contacting streams by plotting the stream temperatures against total heat flow. (Occasional publications also show instead of heat flow either length [10], or heat transfer area [11].) Because the direction of heat flow is arbitrary some authors show increasing temperatures toward the left [12, p. 97], but in this work the cold end is selected as an arbitrary reference for zero and temperature increases to the right (as in [12, p. 123], [13], and [14]), in the same direction as an isobar of a temperature vs enthalpy plot.

If the cold stream transfers heat to a third stream and so on, then these can also be plotted by selecting a different reference heat flow value, so that for example, the exhaust stream, the heat transport loop, and a boiler would appear as three curves, though the total heat transferred in the HRHX may be greater than the total heat transferred in the generator because of transport losses. A conceptual example is provided in Figure 3. Pinch point refers to the pair of points where two curves at the same value of $\dot{Q}$ are in closest approach on the temperature axis [12, p. 97].

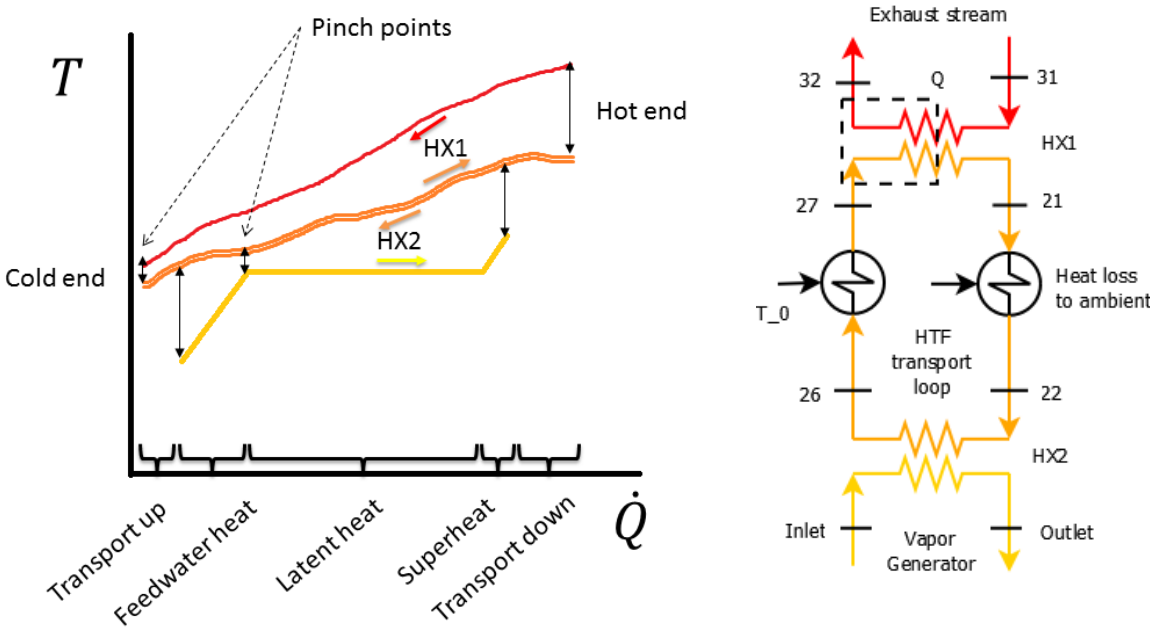

Figure 3. Sequential heat exchange example and plot concept.

Another technique employed by Nishio [15] also documented by Boehm [16] is to rescale the temperature axis to the Carnot cycle factor $(1 - T_0/T)$, which indicates exergy destruction in the area between curves and suggests that the pinch point should be kept toward the cold end or that a gradient in U-value increasing toward the cold end should be arranged, as was analytically shown by Bejan [17]. However, for the most part, the following results will be plotted using temperature directly in order to visualize all heat transfer processes simultaneously (cf. [7]). For convenience, instead of power, enthalpy is used for the horizontal axis, using the refrigerant stream as a reference. Equivalence for any other stream B on the horizontal axis is defined by matching heat flow, using the relation

$$\frac{d}{d\dot{Q}}\dot{m}_{refrigerant}h_{equiv} = \frac{d}{d\dot{Q}}\dot{m}_B h_B. \quad \textbf{(1)}$$

Assuming mass flow is constant throughout the stream, this can be satisfied with a linear rescaling of enthalpy such as

$$h_{equiv} = \frac{\dot{m}_B}{\dot{m}_{refrigerant}}h_B + h_{B,offset} \quad \textbf{(2)}$$

where $h_{B,offset}$ is chosen so that $h_{equiv} = h_{refrigerant}$ at the cold end of the heat exchanger.

In a different context, a related technique is to plot the process heat demand in the form of a grand composite curve, showing cumulative heat requirement as a function of temperature [18, pp. 334-335], but, for convenience, with the same orientation of axes as for a heat transfer plot. Figure 4 shows a hypothetical example representing the demand characteristic of two boilers and one low temperature cooling load, which does not correspond to the application focus of this work. Similarly, one can use this type of curve to represent a heat source or a combination of heat sources distributed over a range of temperatures.

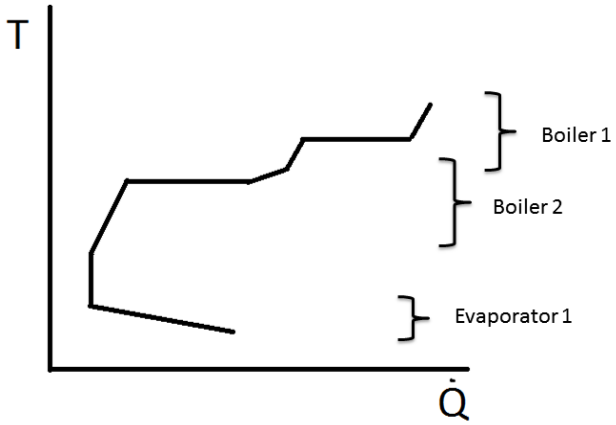

Figure 4. Hypothetical example of a grand composite curve for process heating and cooling demand.

2.2.3 Heat transfer models

In this work, the goal for the analysis of heat transfer processes is to use the simplest possible model that includes the ability to impose a cost constraint and also capture the effects of thermal resistance, which can impact the optimization of flow rates and internal temperatures. Thus, for non-contacting heat exchangers, the UA-LMTD method is applied as described in [19].

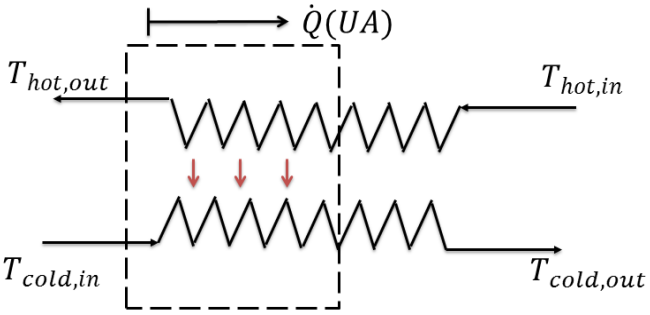

Figure 5. Flow schematic of non-contacting heat exchanger.

In this method, for an individual heat exchanger, the product of overall heat transfer coefficient U and area A are collectively specified as a parameter UA. If each fluid satisfies the assumption of constant specific heat or temperature through the entire exchanger and no dissipation occurs nor work is applied, then the heat flow can be reduced to

$$\dot{Q} = UA\Delta T_{LM} \tag{3}$$

where the log-mean temperature difference (LMTD) is defined for counterflow configuration shown in Figure 5 as

$$\Delta T_{LM} \coloneqq \frac{\Delta T_{hot\ end} - \Delta T_{cold\ end}}{\log R}, \tag{4}$$

$$R \coloneqq \frac{\Delta T_{hot\ end}}{\Delta T_{cold\ end}}, \qquad \begin{cases} \Delta T_{hot\ end} \coloneqq T_{hot,in} - T_{cold,out}, \\ \Delta T_{cold\ end} \coloneqq T_{hot,out} - T_{cold,in}. \end{cases} \tag{5}$$

The non-dimensional parameter R is useful as an indication of how well the stream capacities are matched, since for purely sensible transfer, it is also true that

$$\dot{Q} = \dot{m}_{hot}\left(h_{hot,in} - h_{hot,out}\right) = \left(\dot{m}c_p\right)_{hot}|\Delta T_{hot\ stream}| \tag{6}$$

$$\dot{Q} = \dot{m}_{cold}\left(h_{cold,out} - h_{cold,in}\right) = \left(\dot{m}c_p\right)_{hot}\Delta T_{cold\ stream} \tag{7}$$

Therefore the familiar ratio of stream capacities $S \coloneqq \left(\dot{m}c_p\right)_{cold}/\left(\dot{m}c_p\right)_{hot}$ can be expressed as

$$\begin{aligned} S &= \frac{T_{hot\ in} - T_{hot\ out}}{T_{cold\ out} - T_{cold\ in}} \\ &= \frac{(T_{hot\ in} - T_{cold\ out}) - (T_{hot\ out} - T_{cold\ in})}{T_{cold\ out} - T_{cold\ in}} + 1 \\ &= \frac{\Delta T_{LM}}{\Delta T_{cold\ end}} \log R + 1. \end{aligned} \tag{8}$$

This equation makes clear that S and R have the same inequality relationship with unity, in other words for sensible heat transfer the following classes of equivalent statements arise:

$$\begin{aligned} \left(\dot{m}c_p\right)_{cold} < \left(\dot{m}c_p\right)_{hot} &\Leftrightarrow S < 1 \Leftrightarrow R < 1 \\ \left(\dot{m}c_p\right)_{cold} = \left(\dot{m}c_p\right)_{hot} &\Leftrightarrow S = 1 \Leftrightarrow R = 1 \\ \left(\dot{m}c_p\right)_{cold} > \left(\dot{m}c_p\right)_{hot} &\Leftrightarrow S > 1 \Leftrightarrow R > 1 \end{aligned} \tag{9}$$

There are several reasons for defining R. First, note that S indicates which stream has greater capacity, which by inspection is also the end on which the pinch point occurs. In case purely latent transfer occurs on one side, S is not well-defined, but R continues to indicate which side of the exchanger has the pinch point. Secondly, a naïve implementation of the LMTD method can cause a numerical overflow issue when taking the logarithm of R near unity. In this modelling activity, it is anticipated that the relative capacities of streams in heat exchange may not be known a priori, and so R should be allowed to cross over unity without numerical issues. Therefore as $\delta \coloneqq R - 1$ approaches asymptotically to zero, the following familiar expansion is utilized:

$$\log(1+\delta) \simeq \delta - \frac{\delta^2}{2} + \frac{\delta^3}{3} - \frac{\delta^4}{4} + \frac{\delta^5}{5} - \frac{\delta^6}{6} \tag{10}$$

$$\begin{aligned} \Rightarrow \Delta T_{LM} &= \Delta T_{cold\ end} \frac{(R-1)}{\log R} \\ &\simeq \Delta T_{cold\ end} \frac{\delta}{\left(\delta - \frac{\delta^2}{2} + \frac{\delta^3}{3} - \frac{\delta^4}{4} + \frac{\delta^5}{5} - \frac{\delta^6}{6}\right)} \\ &= \Delta T_{cold\ end} \left(1 - \frac{\delta}{2} + \frac{\delta^2}{3} - \frac{\delta^3}{4} + \frac{\delta^4}{5} - \frac{\delta^5}{6}\right)^{-1}. \end{aligned} \tag{11}$$

Third, R can be used as a non-dimensional means to describe the shape of the gap between the temperature-heat curves. In contrast, a conventional specification for chiller water is to fix the temperature rise on one side of the fluid at 5 °C. Specifying R instead allows the exergy destruction from finite heat transfer to be made arbitrarily small as the UA value is increased.

There are several cases where the heat flow curve does not meet the requirements for use of a single LMTD equation. Notably, boilers that provide feedwater heating or superheating violate the assumptions outlined above. For these components it is possible to use an LMTD method by employing separate LMTD equations for each regime of flow, as long as specific heat is fairly constant in the

superheated range. However, in this work, feedwater heating and superheat are usually small contributions to the total heat input, and thus following on Herold et al. [12] these are neglected in terms of contributions to required heat exchange area. The fraction of these heat contributions are nevertheless observed in the results, and the use of a detailed model is suggested for future work. Similar justification is allowed for neglecting area required for heat transferred to non-saturated states in condensers and evaporators.

2.2.4 Constraints, objective function, and optimization technique

Any optimization problem requires specification of constraints and objective function. In the development of this work, several options were considered for constraining the costs related to heat transfer. First, the concept of a common value for pinch point temperature differences was applied. Later, in keeping with [12], a total was specified for all heat exchangers except those internal to the chiller. Results for both types of constraint are informative and presented here, but technology comparison is based on the second type.

The objective function is cooling capacity. In the following, optimal configurations are presented as a function of ambient temperature. The optimization could be performed using a seasonal average cooling capacity, with weighting for multiple values of ambient temperature. However, the computational cost is lower for optimization to a single ambient temperature, and the technique is in keeping with ASHRAE standards for design load conditions as discussed in [20]. It makes sense to choose for a given site a single ambient temperature for design point optimization, then follow-up with a study of performance at off-design conditions likely to be experienced. Heat rejection system and data for ambient conditions will be discussed in the next chapters.

2.3 Water ejector cycle

2.3.1 Ejector cycle methods and assumptions

The long history of ejector pump usage for cooling is discussed in [21]. It has evidently fallen out of favor for building conditioning due to low efficiency but remains in use for some applications where other factors make it preferred. As shown schematically in Figure 6, the ejector cycle is analogous to the vapor compression cycle but uses an ejector pump in place of a compressor. Inside the ejector pump, a nozzle converts a high pressure and high temperature motive stream into a low pressure, high velocity stream. The high velocity stream draws in and mixes with refrigerant vapor from the evaporator. The mixture consumes its remaining kinetic energy to diffuse up to medium pressure for condensing heat rejection. The stream is then split into two streams, one of which is compressed back to the high pressure and returned to the boiler (called here a vapor generator) to receive the driving heat input, and the other is passed through an expansion valve and delivered to the evaporator to receive the heat input from the load. In some cycles, the motive fluid and refrigerant are the same fluid; in other cycles, a separator is added to the cycle. In this preliminary analysis we use water for both streams. The heat exchangers are depicted schematically in Figure 7, and the internal state points are described in Table 1.

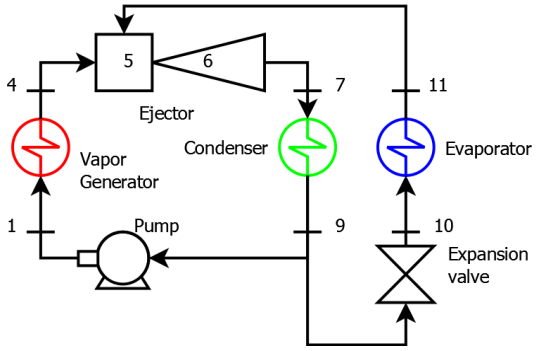

Figure 6. Ejector cycle process. The components on the left form a power cycle that acts as the compressor for the refrigeration cycle, with shared condenser.

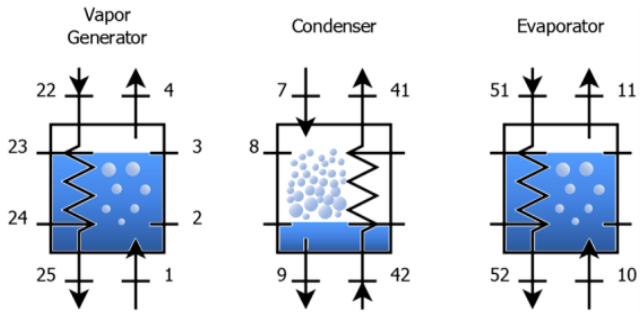

Figure 7. Schematic for heat exchangers in ejector cycle.

Table 1. Ejector cycle internal state points.

Index	Stream	Phase	Description
1	Motive	subcooled	Compressor exit/boiler inlet
2	Motive	sat liquid	Boiler internal point
3	Motive	sat vapor	Boiler internal point
4	Motive	superheated	Boiler exit/nozzle inlet
5	Motive	two-phase	Nozzle exit prior to mix
6	Both	two-phase	Mixed streams at high pressure
7	Both	superheated	Diffuser outlet/condenser inlet
8	Both	saturated vapor	Condenser internal point
9	Both	saturated liquid	Condenser exit/pump & throttle inlets
10	Refrigerant	two-phase	Throttle exit
11	Refrigerant	saturated vapor	Evaporator exit

The model used in this analysis follows mainly from [22], [23], and [24]. A key assumption is that the ejector pump is characterized by three coefficients, called the nozzle efficiency, entrainment efficiency, and diffuser efficiency, which are related to the fractions of kinetic energy used up in the successive cross-sections through the ejector. Other models use different sets of coefficients, which all tend to be

determined experimentally [25]. A future work should be to analyze the validity of the assumption that these efficiencies can be satisfied by some physical design at the given design point. Additionally, some state points are assumed to lie on saturation curves, as can be seen in the plots in the results section. This assumption varies between different modeling approaches in the literature, depending on whether the diffuser is designed to exhibit a condensation shock in which two-phase flow occurs. Other pumps are designed for vapor-only states throughout the entire pump and thus operate at higher temperatures for the same three pressure levels. For the generator, this implies a higher availability heat source is required, etc., so it may be hypothesized that an ejector pump should operate as close as possible to the saturated vapor curve.

Following [24] in which water was the fluid in both streams, the coefficients characterizing the ejector pump performance in the model are fixed as shown in Table 2. Also note that an earlier work using these three coefficients specified higher values [22]. Finally, note that kinetic energy is assumed to be negligible except at states 5 and 6.

Table 2. Ejector pump model coefficients and values for water as a working fluid.

Coefficient name	**Value**
Nozzle efficiency, η_{nozzle}	0.85
Mixer efficiency, η_{mixer}	0.70
Diffuser efficiency, $\eta_{diffuser}$	0.70

The nozzle efficiency η_{nozzle} is defined as a ratio of actual kinetic energy relative to that resulting from an isentropic expansion to an artificial state 5' as

$$\eta_{nozzle} \coloneqq \frac{KE_5}{KE_{5'}} = \frac{h_4 - h_5}{h_4 - h_{5'}}, \tag{12}$$

where the second equality is a result of the steady-state energy equation with no other forms of energy present and no change in mass flow rate. The state points refer to Figure 6. Thus the nozzle model automatically satisfies the second law. The entrainment efficiency $\eta_{entrainment}$ is defined as the fraction of kinetic energy *KE* preserved in the stream through the mixing section:

$$\eta_{entrainment} = \frac{\dot{m}_6 KE_6}{\dot{m}_5 KE_5}. \tag{13}$$

Note that this is distinct from the entrainment ratio of mass flow rates, $\lambda \coloneqq \dot{m}_{refrigerant}/\dot{m}_{motive}$, which although a useful indicator of pump operation, is not an input in this model.

The diffuser efficiency $\eta_{diffuser}$ is also a so-called isentropic efficiency, where 7' is an artificial state that would result from isentropic expansion from state 6,

$$\eta_{diffuser} = \frac{h_{7'} - h_6}{h_7 - h_6} \tag{14}$$

As a result, lower $\eta_{diffuser}$ indicates a need for higher kinetic energy at state 6, etc.

In addition to the state point constraints and given values for the three coefficients, mass and energy balance equations are imposed for each of the components, and for each heat exchanging component, a heat transfer equation is used as described above to couple the heat flow and temperatures of the internal and external streams.

2.3.2 Ejector system modeling results

The single stage ejector cycle with water as both motive fluid and refrigerant was modeled. Figure 8 shows a typical result of the state-space representation of the process with overlaid heat exchanger plots using the method described in section 2.2.2. Dashed lines indicate the external flows. Note that generator (transferring heat from HTF, 22→23→24→25, to motive stream, 1→2→3→4) has pinch where point 24 heats point 2.

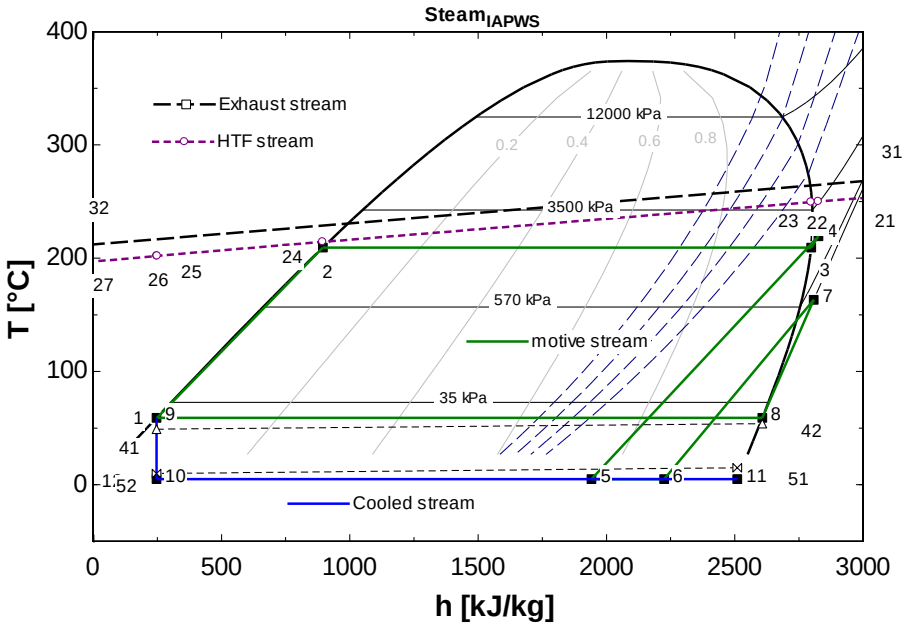

Figure 8. Ejector cycle typical process in state-space representation of ejector cycle

Figure 9 shows the trends of COP and rate of heat input at different levels of ambient temperature, plotted against the generator internal saturation temperature, T_3. Note that generator saturation temperature is determined by the control set-point for pumped internal mass flow rate. The trend with respect to heat input temperature agrees with existing works by Untea et al [26]. The trend with respect to heat rejection (or ambient) temperature (more clearly shown in Figure 12) agrees with other existing works such as Dennis and Garzoli [27]. While the heat input is fairly constant with respect to ambient temperature, the COP is quite sensitive. This is in part a result of the increasing requirement for kinetic potential energy at point 6 (decreasing entrainment rate) for the diffusing mixture to return to an

increasing condenser pressure at point 7. Meanwhile, cooling effect supplied by each unit of mass through the evaporator also decreases because of the increasing vapor fraction at point 10.

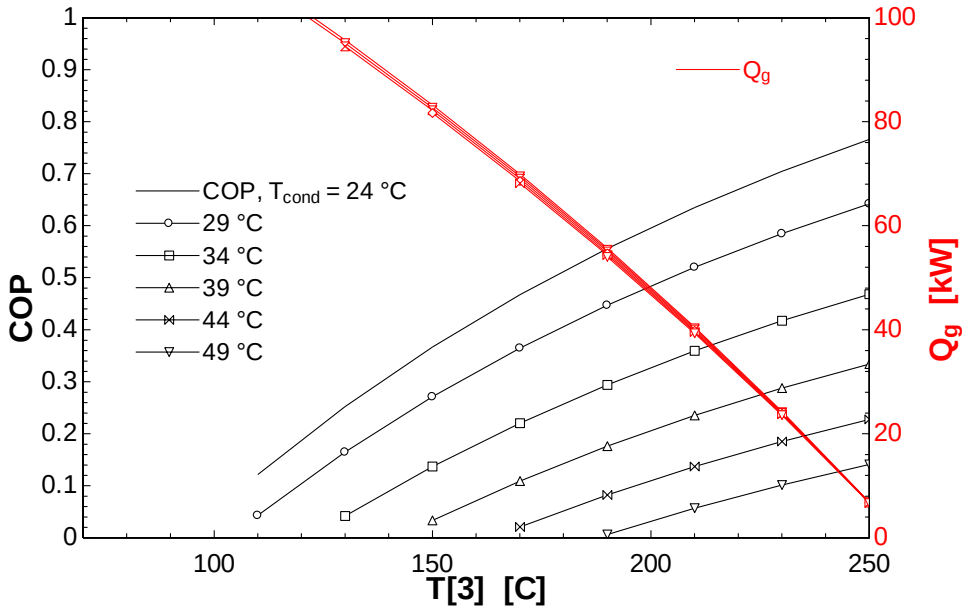

Figure 9. Inverse trends of COP and generator heat input for different levels of ambient temperature (indicated for each curve). The x-axis is the generator saturation temperature.

Figure 10 shows the cooling rate (which is the product of the curves in the previous figure) plotted against generator internal saturation temperature, T_3, for different levels of ambient temperature. The result shows that there is an optimal generator saturation temperature to maximize cooling rate as a function of ambient, as shown by the dashed line.

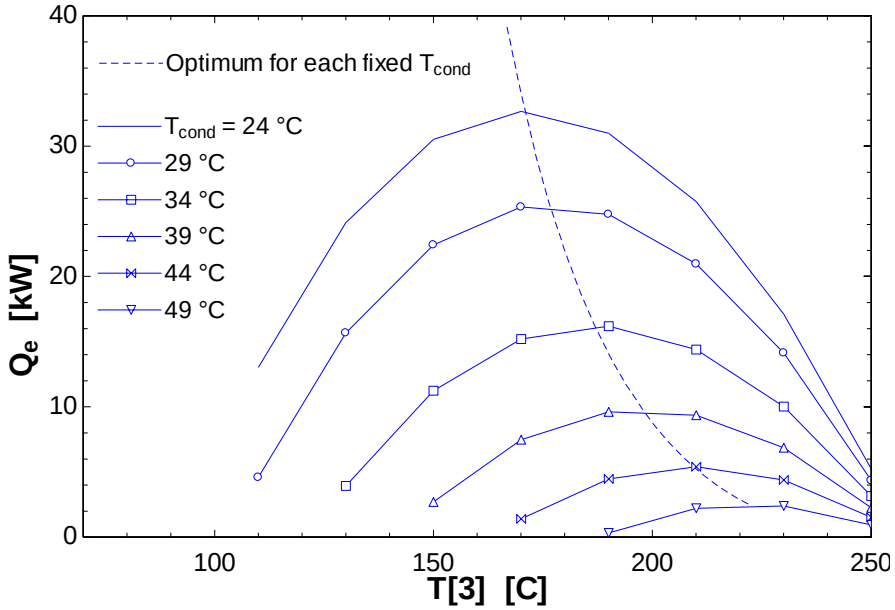

Figure 10. Optimum design of generator temperature.

Again, the curves in Figure 9 and Figure 10 are not merely the result of calculations for fixed design parameters, but an optimization subject to constraints. Figure 11 shows the optimal allocation of heat exchanger areas subject to a constrained total and an input generator saturation temperature. The constraint for heat exchange area is equivalent to the result from a base case of $\Delta T_{HX,typical} = 5\ \mathrm{K}$ (using a catalog or fixed ratio approach not discussed here) and an ambient temperature of 39 °C, which is 16.61 kW/K. The optimized allocation is not uniform and not constant with respect to ambient temperature. The results fairly well agree with the prediction regarding the order of pinch point temperature differences for a given ambient temperature.

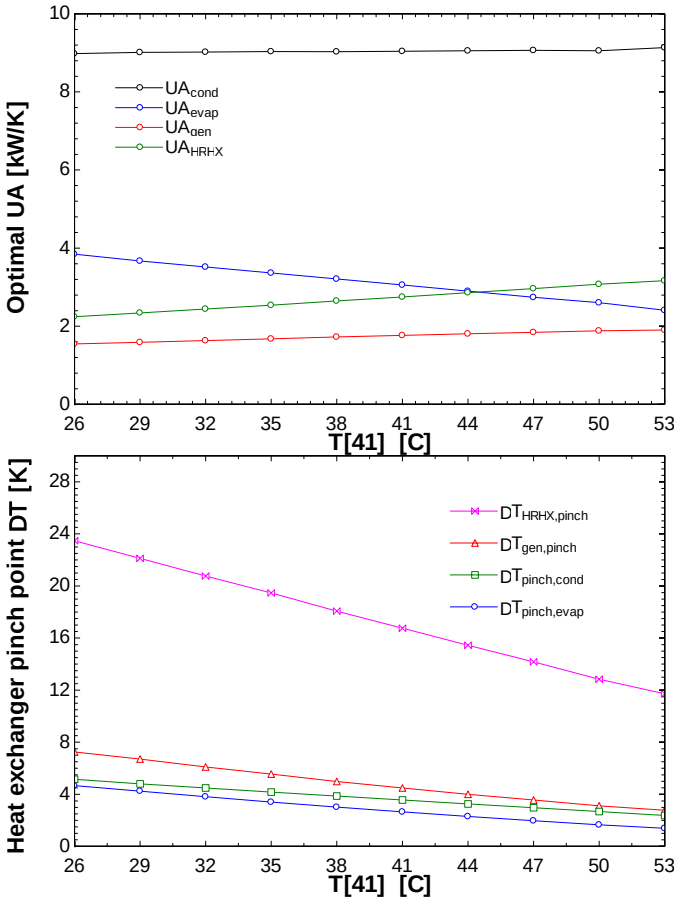

Figure 11. Dependence on ambient temperature of optimal allocation of heat exchanger area to maximize cooling capacity, with total UA of 16.61 kW/K.

Figure 12 shows an alternate projection of the results with ambient temperature on the horizontal axis and varying iso-curves for total value of heat exchange area. These results are discussed more in the comparison in a following section.

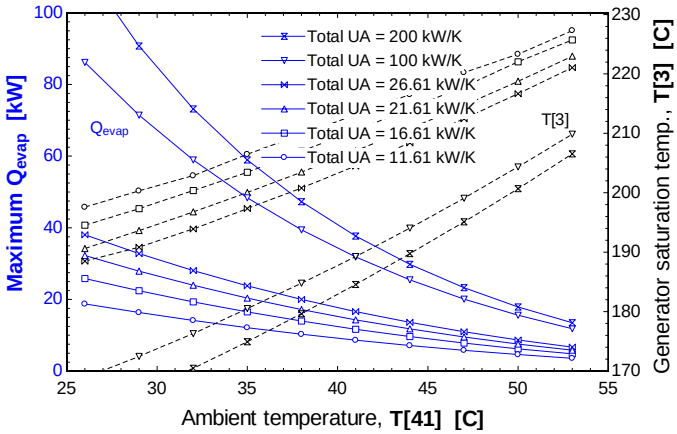

Figure 12. Area-constrained optimization of cooling capacity by varying allocation of heat exchange surface area. Solid curves show maximum cooling capacity and dashed curves show optimal generator saturation temperature. The variation with ambient temperature, for various levels of total UA, is shown.

2.4 Single-effect lithium-bromide absorption cycle

2.4.1 Absorption cycle methods and assumptions

The absorption cycle has a long history of use for cooling, and cycle design and modeling techniques and assumptions are described by Herold et al. [12]. In this particular cycle, aqueous LiBr is the absorbent and water is the refrigerant. Absorption is exothermic and desorption is endothermic; this is the basis for using heat input to drive vapor generation. In order to model the rates of evaporation from and condensation into solution, we assume that liquid and vapor are at equilibrium at the surface, meaning equality of pressure, temperature, and component Gibbs free energies. From this assumption and the reaction energy, a relation may be obtained between equilibrium vapor pressure of water above a solution and the solution's temperature and LiBr mass concentration. The solution circulates in a loop between a generator and absorber, in which components heat is exchanged to the surroundings in counterflow to the liquid solution. In the high temperature and high pressure generator or desorber, heat input drives boiling of a fraction of the water from a circulating solution. In the low-temperature and low-pressure absorber, heat from absorption is rejected. In these devices, simultaneous mass transfer occurs to a vapor stream which flows through the cooling circuit to condenser, expansion valve, and evaporator.

For the simplest possible model that provides relation between size, performance, and external temperatures, a steady-state model was employed for the design shown schematically in Figure 13. Additional internal heat exchangers can be added to increase performance under some conditions, but this single-effect cycle with solution heat exchange performs reasonably well over a range of external temperatures. The equations for modeling this process at steady state at a component level are simply mass, concentration, and energy balances, with the addition of the liquid-vapor equilibrium imposed in the generator and absorber, all documented by [12] in sufficient detail to reproduce, including pump efficiency. The only component requiring some clarification is the generator, in which the solution inlet is a subcooled state, meaning there is a portion of heat exchange to raise the stream enthalpy up to a

saturated state, as visualized in Figure 14. Table 3 lists the state point descriptions and assumptions. Some points have been added to indicate saturated states that are not otherwise required to solve the model.

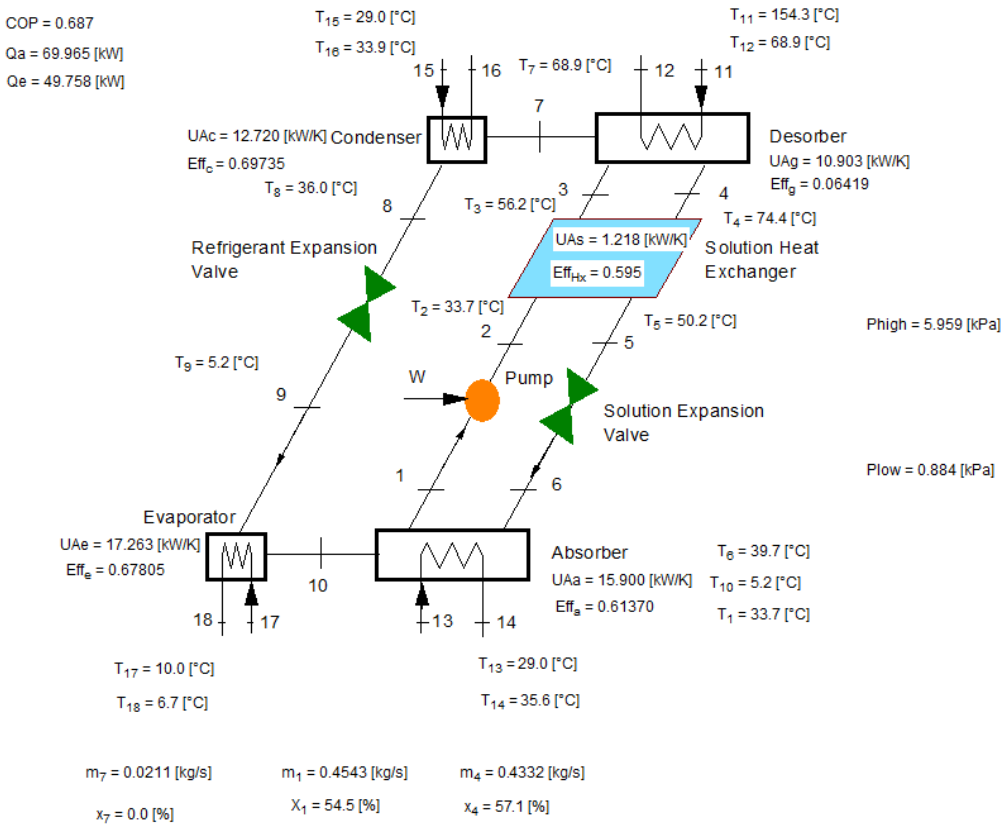

Figure 13. System schematic with LiBr single effect chiller. Based on original diagram from [12]. [TODO: update state point indices.]

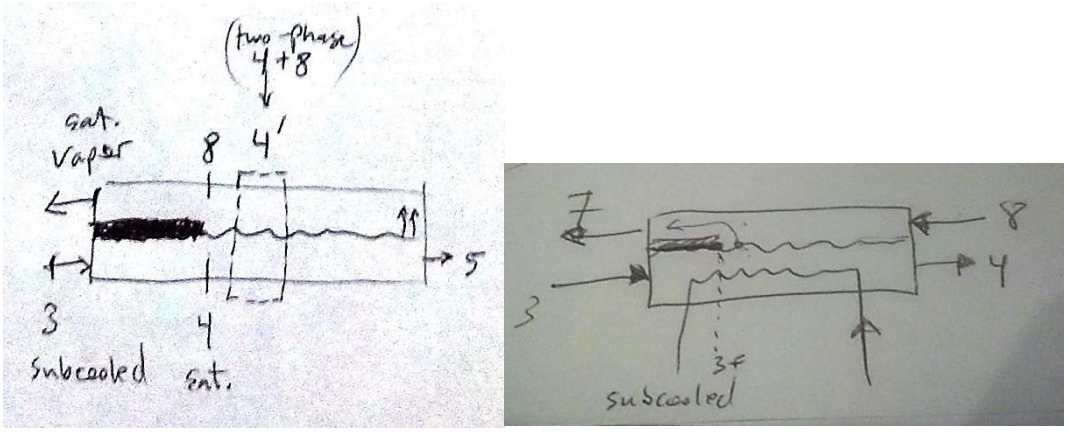

Figure 14. Liquid and vapor streams in generator. States 4 and 8 are in equilibrium, and external heat exchange occurs with liquid stream.

Table 3. State point assumptions for LiBr single-effect chiller model.

Index	Stream	Phase	Description
1	Weak solution	Saturated liquid	Absorber solution outlet
2	Weak solution	Subcooled liquid	Solution pump outlet
3	Weak solution	Subcooled liquid	Solution heat exchanger outlet
4	Weak solution	Saturated liquid	Generator internal point
5	Strong solution	Saturated liquid	Generator outlet
6	Strong solution	Subcooled liquid	Solution heat exchanger outlet
7	Strong solution	Two-phase mixture	Solution expansion valve outlet
8	Refrigerant	Superheated vapor	Generator outlet
9	Refrigerant	Saturated vapor	Condenser internal point
10	Refrigerant	Saturated liquid	Condenser outlet
11	Refrigerant	Two-phase mixture	Expansion valve outlet
12	Refrigerant	Saturated vapor	Evaporator outlet

Crystallization of LiBr presents a challenge for system design and control. The limitations of solubility are given in [12] as a relation between LiBr concentration and temperature. From this relation, an equivalent representation in the vapor pressure-temperature plane may be computed, which is useful since the cycle is often visualized with this projection, referred to as a Dühring diagram. Some additives have been shown to reduce the risk; other techniques that may be used are dilution of absorber solution when a high concentration and temperature is detected, as done by York (todo cite), and use of scraped surface heat exchanger.

2.4.2 Absorption cycle modeling results

There are many results, as shown in Figure 15, Figure 16, and Figure 17.

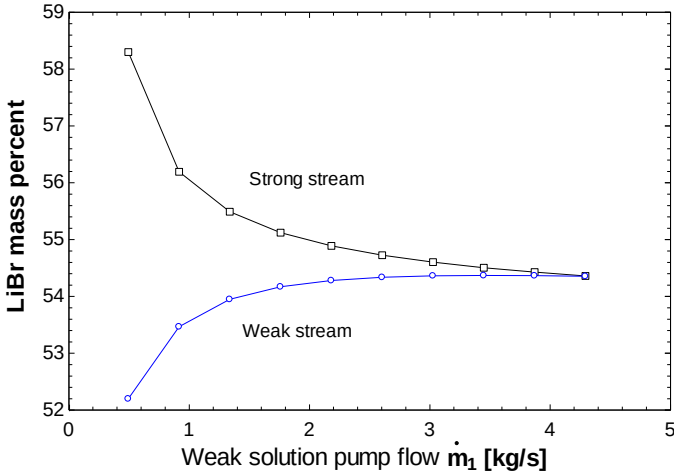

Figure 15. The concentration in the two streams varies with flow rate. When the flow rate is very high, the concentrations are equal, setting an upper limit for flow rate in the plots for this section.

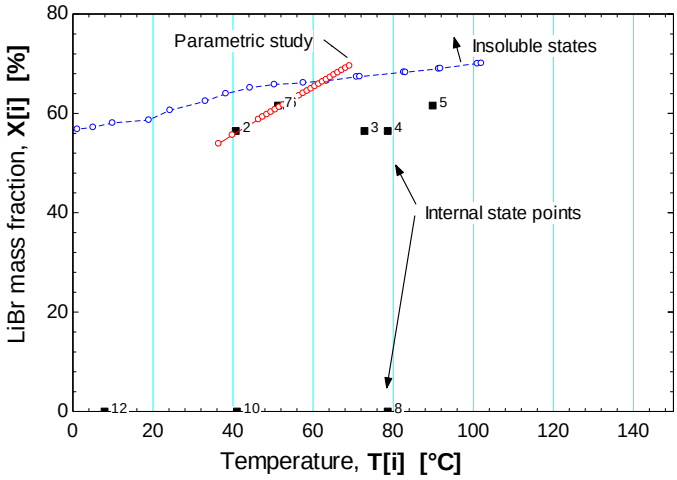

Figure 16. Running the solver updates this depiction of the internal state points as a check for crystallization against the solubility limit given in [12]. This was used to establish the crystallization limits in Figure 17.

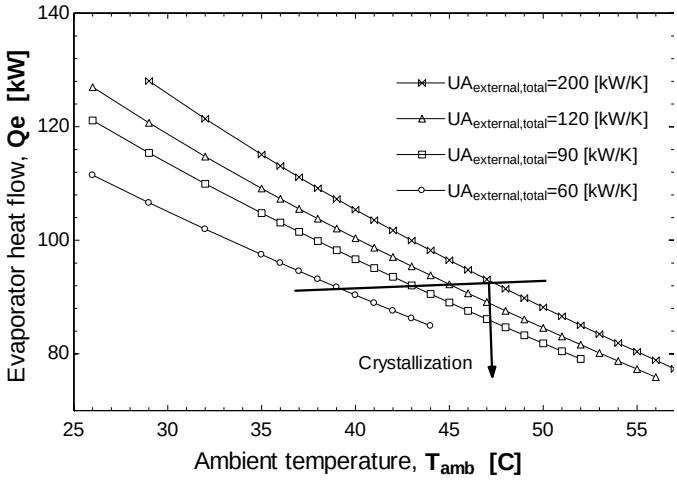

Figure 17. For each shown value of chiller designed with the catalog method and optimum pump rate, the variation of cooling capacity with ambient temperature is shown. For high ambient temperatures, the expanded strong solution crosses the crystallization boundary. (This could be mitigated by adding heat to that stream, requiring additional heat rejection and decreasing performance.)

2.5 Single-effect ammonia-water cycle

The assumptions for the ammonia-water cycle are basically the same as for the lithium bromide cycle, except for the addition of a rectifier and a condenser-evaporator heat exchanger, as in the simplest case model considered by Herold et al. [12] in their example 9.3. Table shows a list of internal state point descriptions, and Figure 18 shows the EES model diagram and some outputs.

Table 4. Internal state points for ammonia-water absorption cycle

Index	Stream	Phase	Description
1	Rich	…	…
2	Rich	…	…

3	Rich	sat vapor	…
3’			…
4	Weak	superheated	…
5	Weak	two-phase	…
6	Weak	two-phase	…
7	Rectifier	saturated vapor	…
8	Rectifier	saturated liquid	…
9	Refrigerant	saturated vapor	…
10	Refrigerant		…
11	Refrigerant	saturated vapor	…
12	Refrigerant		
13	Refrigerant		
14	Refrigerant		

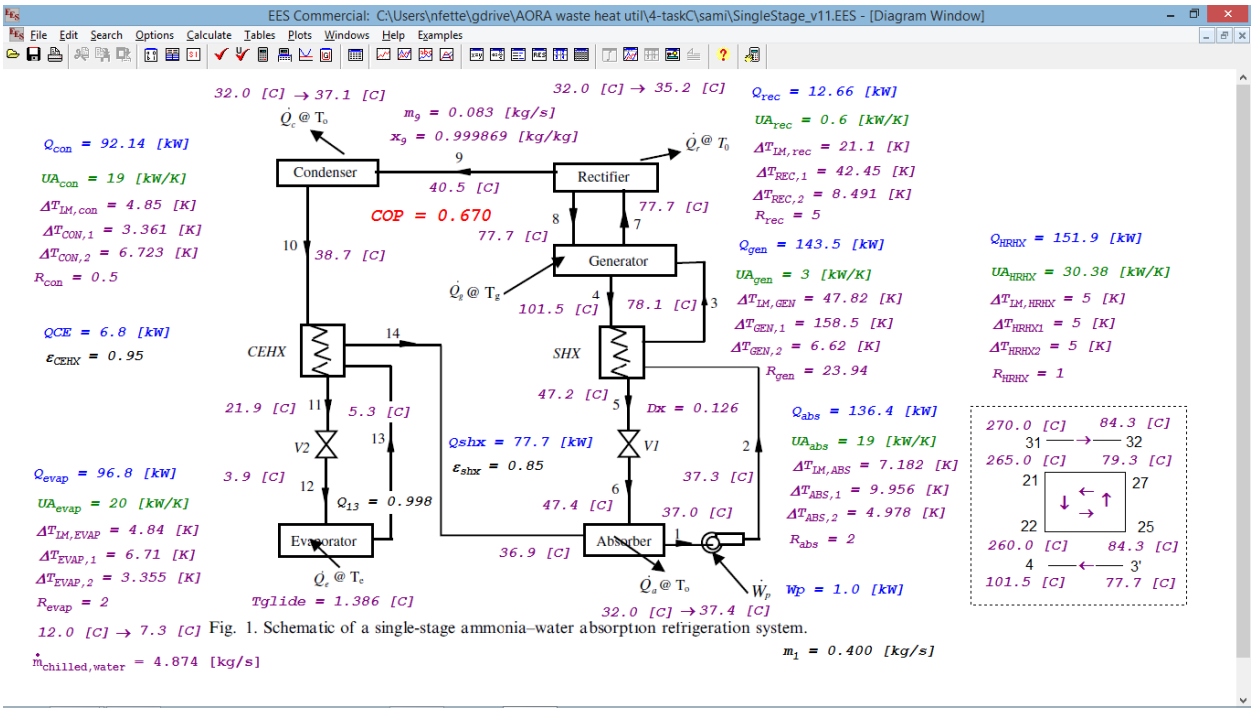

Fig. 1. Schematic of a single-stage ammonia–water absorption refrigeration system.

Figure 18. Cycle diagram of a simple single-effect ammonia-water absorption cycle. The box on right indicates the heat recovery and transport loop.

2.5.1 Pumped flow rate parameter study

A notable difference from the lithium bromide cycle is that in the ammonia-water cycle, the generator internal minimum temperature shows much less sensitivity to changes in pumped flow rate. This can be seen through a parametric study (file: SingleStage_v11.EES) in which only pumped solution mass flow is varied, and no optimization is performed. Figure 19 shows the concentration of the solution streams and that rich solution (eg, point 3, which determines the concentration in equilibrium with the rectifier

streams) is at nearly constant concentration. (Compare Figure 15 for the LiBr cycle in which both streams vary in concentration.)

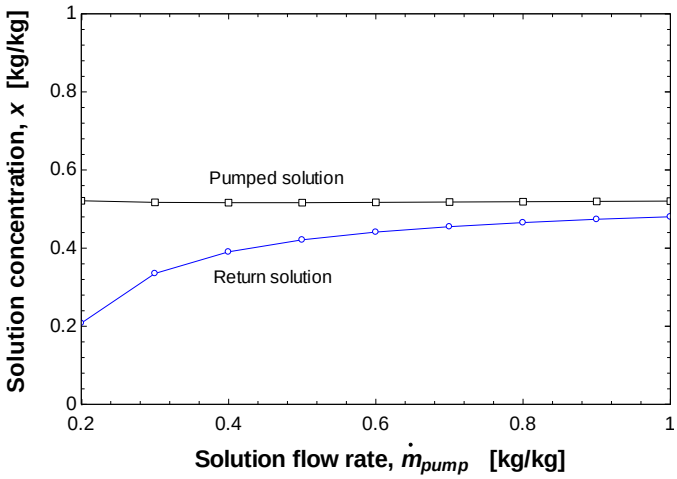

Figure 19. The concentration in the solution streams varies with pumped flow rate.

Figure 20 shows the corresponding internal temperatures and resulting COP. The generator internal temperatures are coupled to the heat supply. This can be seen in the generator heat input curve in Figure 21, which also shows the other heat flows. The evaporator heat input can be seen to have a maximum where solution pumped flow rate is around 0.4 kg/s, which is the base case shown in more detail in Figure 18.

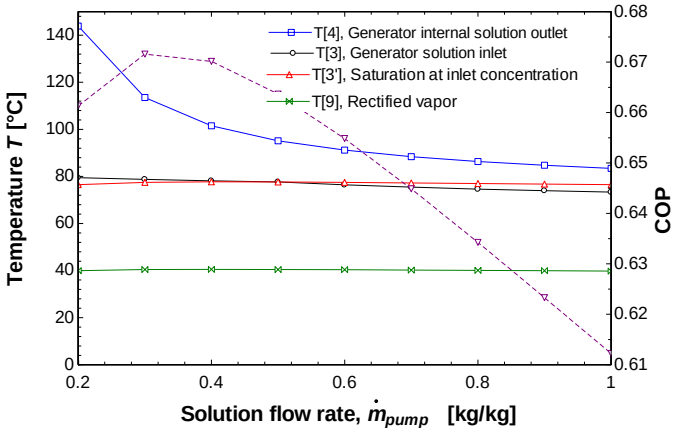

Figure 20. Stream temperatures in single effect ammonia-water parametric study.

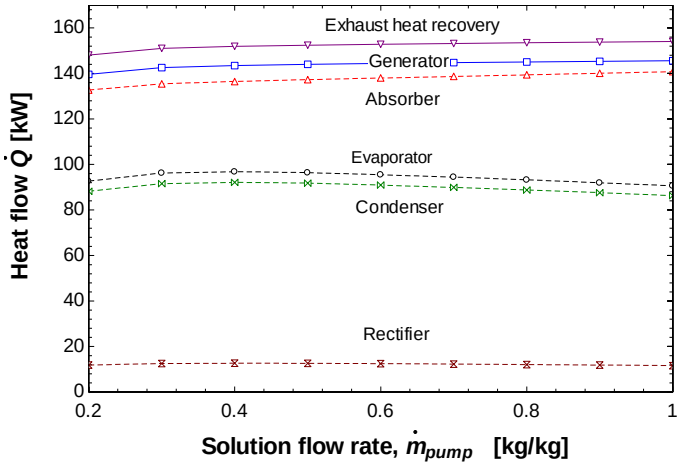

Figure 21. Heat flows for the single parameter study of a simple single-effect absorption cycle with ammonia-water.

2.5.2 Optimization results

The same optimization process as used before was applied to the ammonia-water model (file: …).

figure pending

Figure 22. Some optimization results for ammonia-water absorption cycle model.

2.6 Cooling technology comparison

Figure 23 shows a comparison of the results from the completed modelling efforts discussed in the previous sections. It indicates that, with sufficient chiller size (in terms of heat exchange area), a LiBr single effect absorption chiller produces much more cooling capacity than an ejector cooling cycle with water. However, due to the crystallization limit, the absorption chiller does not operate at very high temperatures for heat rejection, and the threshold for operation decreases as the chiller size is reduced. (This last result is true for the optimized result; however, it may be possible to operate the chiller away from the optimal set-point by adjusting pumped mass flow rates, for instance.)

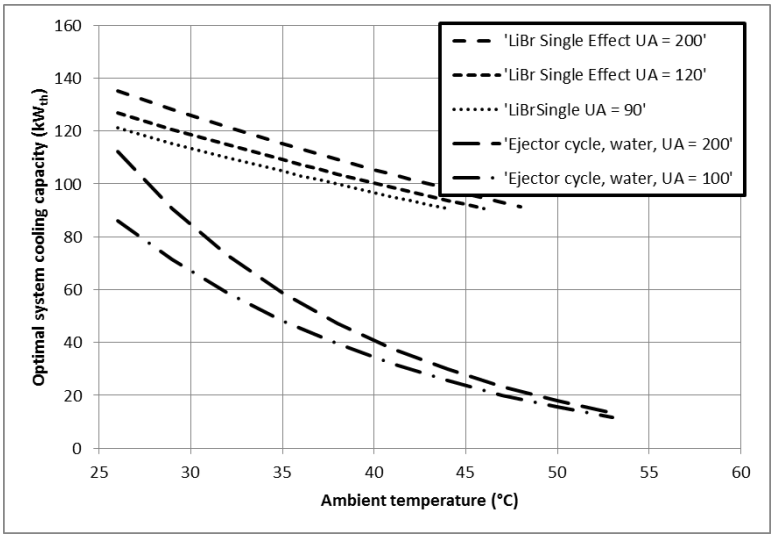

Figure 23. Cooling capacity comparison between technologies at several levels of cost proxy.

2.7 Conclusions and future work

In addition to the cycles reported so far, a number of other technologies should be compared, including double-effect lithium bromide absorption cycles; ammonia-water absorption cycles; and ejector cycles with other common refrigerants. Adsorption cycles may be also compared; though they have typically lower performance than lithium bromide absorption cycles, they may have higher limits on temperature for heat rejection. Solid and liquid desiccant cycles are not preferred because significant water consumption is common among these technologies.

For the ejector cycle model, a number of further steps may be taken. To determine uncertainty or a range of possible operation conditions, a number of different variations on the ejector cycle model could be employed, such as outlined in [25]. Indeed, the results from the model used in this work are subject to the assumed coefficients. The influence of the assumed ejector pump coefficients could be assessed by a sensitivity analysis, such as by varying them over a range from 0.5 to 1.0, for example, and observe the relative distribution of COP and cooling capacity results for a given ambient temperature, in a manner similar to that presented in [28]. Additionally, treating the coefficients as constants over the full range of operation may not be an accurate representation of performance when the design pressures are changed significantly, so more detailed performance models should be found as future work to refine the model for off-design study. A useful reference for continued work would be an older edition ASHRAE Handbook of Equipment (eg [29], cited in [30]). In the 2012 Handbook of HVAC Systems and Equipment, the term ‘steam jet’ never appears, and the word ejector appears only six times, mostly in passing comments [31].

3 Heat rejection system selection and water usage control

3.1 Introduction and purpose

In some locations, the economic and environmental costs for water consumption are high enough to merit conservation but are not prohibitive, in which case the designer should ask what is the most effective heat rejection system. The previous chapter made no assertion about the heat rejection system but took as an input the effective temperature available for heat rejection, so that the conclusions from this chapter may be incorporated with little change into the design approach.

In this chapter, we outline future work to optimize the cooling system when a certain amount of annual water consumption is allowed, and answer the questions: what should be the system level design, component level design, and controls for the allocation of cooling water throughout the year? At the system level, we perform a technology comparison for relevant performance metrics as functions of ambient conditions. For chiller heat rejection we consider dry cooling, direct evaporative cooling, hybrid wet-dry cooling, indirect evaporative cooling, and ground source heat rejection. For inlet cooling we compare conventional spray inlet cooling to chiller-supplied cooling. At the component level, we draw from an on-going work for design, analysis, and construction of an indirect evaporative cooling tower to identify the parameters that may be optimized in the context of multiple objectives for water conservation and cooling system performance and to determine sizing and cost information where published data are insufficient, since the technology remains relatively rare in the market. The controls may be based on real-time ambient conditions and demand and any available information about the annual average distribution of ambient conditions. Given that information, the control algorithm should also be able to demonstrate in simulation the ability to satisfy the water constraint at a given confidence interval.

For a general reference on terms and relation between dry bulb, wet bulb, dew point, humidity ratio, and moisture content, see [32].

3.2 Heat rejection system models

3.2.1 Heat rejection technologies to be included

As discussed in [33], there are several common types of heat rejection equipment.

- A *dry coil* is a non-contacting heat exchanger with air flowing on one side and either condenser fluid or a sensible heat transfer fluid in a transport loop flowing on the other side.
- A *direct evaporative cooling tower* is a direct contacting heat exchanger for water to reject heat and mass to an air stream, resulting in an outlet water temperature that approaches the wet bulb temperature instead of the dry bulb. A typical measure of performance resulting from the cooling effect is the wet bulb effectiveness η_{wb}, or the ratio of temperature reduction from ambient relative to the limit obtained if the temperature were reduced all the way to the wet bulb. Where T_w is the water outlet temperature from the cooling tower, this is

$$\eta_{wb} = \frac{T_{DB} - T_{water}}{T_{DB} - T_{WB}} \quad \textbf{(15)}$$

- An *indirect evaporative cooling tower* can be designed via one of two methods. The first is to use an indirect evaporative air cooler, which in successive stages cools an air stream without increasing its moisture content, and then pass the dry, cool air to the cooling tower. The second is to use a single stage of heat recovery in the form of a recuperator, whereby moist, cool air exiting the cooling tower can precool inlet air, thus reducing its wet bulb. A typical measure of the performance of an indirect evaporative air cooler is the dew point effectiveness η_{dew}, so a similar measure may be useful in the analysis of a water cooling tower:

$$\eta_{dew} = \frac{T_{DB} - T_{water}}{T_{DB} - T_{dew}} \quad \textbf{(16)}$$

- One form of wet/dry hybrid cooling tower is simply a package including both a direct evaporative cooling tower and a dry coil with a valve to allow cooling without water consumption.
- Ground source heat rejection may be accomplished via closed loop piping inserted into deep bore holes. Heat transfer fluid is then pumped through the loop and to the condenser exchanger. The potential for ground source heat rejection varies with geology and climate, but for a given location, the effective temperature or thermal resistance may be related to the volume average heat input rate, and thus field size and cost. This method for heat rejection does not necessarily consume water and offers an alternative for arid locations with cool and hot seasons.

3.2.2 Performance models and metrics

A system selection comparison will follow the approach in which a cost function is constrained and the instantaneous chiller cooling capacity is computed over a range of ambient conditions. As a case study, ambient data for Phoenix, AZ may be used. In comparison to the previous chapter, the cost no longer includes only fixed costs but now includes variable cost, so we cannot make a fair instantaneous comparison. So rather than constraining the fixed cost, we may assume that area is not constrained, but that water consumption determines cooling tower effectiveness and thus effective heat rejection temperature. Similarly, we will search literature on ground source heat rejection in Phoenix, and in other locations for comparison, since such a technique was the winning bid for a large commercial building re-purposing project in the area. Then, having a variety of effective temperatures as functions of ambient temperature and humidity, we can plot the chiller cooling capacity when heat is rejected to that effective temperature. Thus results in a set of 2D surfaces; visualization may be messy, so cross-sections may be useful, such as views of 20% humidity, 40%, etc., with dry bulb on the x-axis and effective temperature and cooling capacity on the y-axis. In the case of ground-source heat rejection, effective temperature is not a function of instantaneous ambient conditions, but may be correlated. The result may then be represented via a min/max range or percentile box plot.

The goals for this work are best explained by an example. Figure 24 shows an example of the kind of information that a model should produce. The information is equivalent to a relation for the minimum

achievable cooling water output temperature over a range of ambient psychrometric states, given a specified rate of water consumption per unit heat rejected.

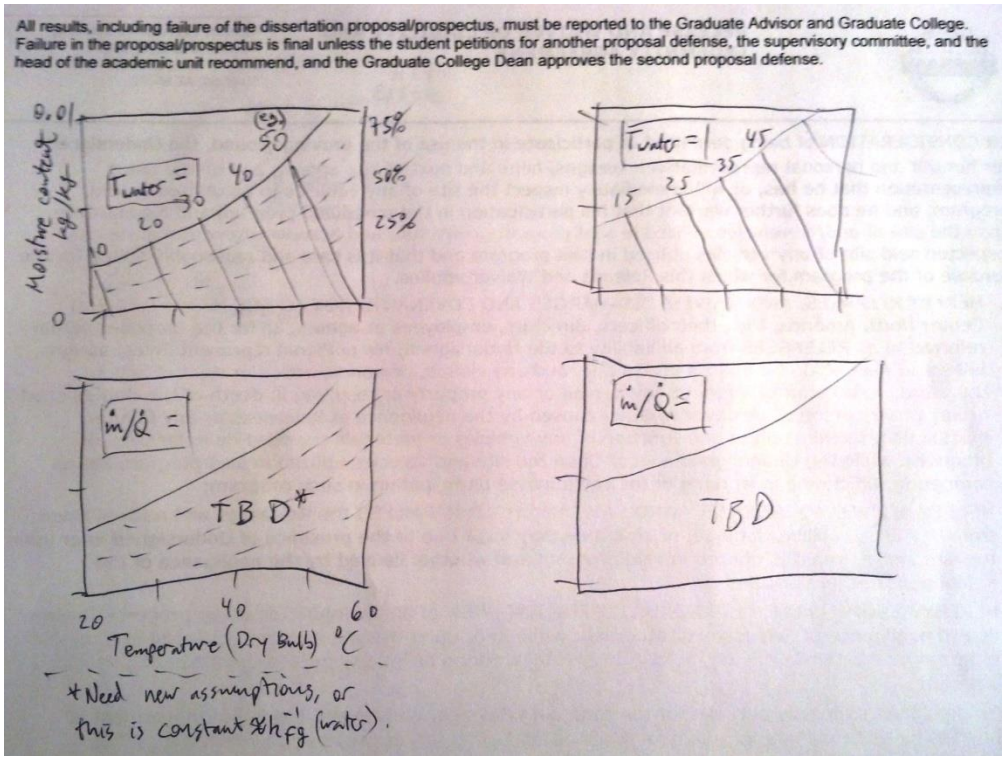

Figure 24. Cooling tower performance: for 50% effectiveness, contours of cooled water outlet temperature and water consumption rate over psychrometric state space for direct (left) and indirect cooling towers (right).

3.2.3 Indirect evaporative cooling tower model

3.2.3.1 Purpose

Although the commercial development of a cooling tower in this category has been disclosed by DesChamps [34], its performance model and tests have not yet been found in the literature. However, the Coolerado air cooler has been well studied and reported in [35], and a suitable air-air recuperator is offered commercially (also by DesChamps) [36].

In this work, we will extend the numerical model of a heat pipe heat exchanger with wet exhaust section, developed for the 2013-2014 Max Tech and Beyond student competition, by including the evaporative media and water in the main portion of the cooling tower. This will result in a model complete enough to describe the relation between air flow rate, water flow rate, ambient inlet state, cooling water inlet state as inputs and cooling capacity and water consumption as outputs. We will also model the second type of indirect cooling tower by combining data from the Coolerado air cooler with a typical model for a cooling tower fed with the dry, cool air.

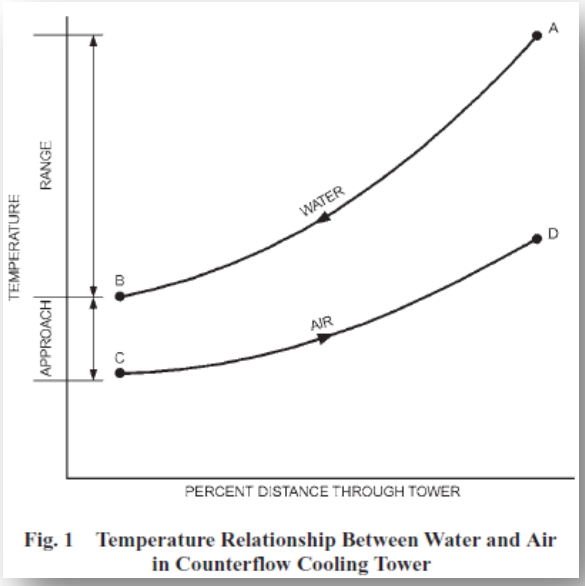

Figure 25. A heat transfer diagram for a direct evaporative cooling tower from ASHRAE [33].

3.2.3.2 Existing work on recuperator based design and model

Student volunteers compiled the necessary mass and heat transfer correlations to build a simple, steady-state model with some guidance and literature supplied by the author. The model is coded in EES and can be used following debugging to provide a physical model for heat rejection via an indirect evaporative cooling tower. For most accurate results, the model needs to be extended to have a discretization of multiple cells inside the cooling tower and recuperator, as the present model treats the convection properties as constant, but it is known that the direction of the process in the psychrometric chart may change from the air inlet to outlet, and so the process should be modeled with multiple cells [37], as shown in Figure 26 and Figure 27. The calculations are also described in [33]. One should note that these are based on the Merkel method in which the Lewis factor giving the relative rates of heat (sensible) to mass (latent) transfer is assumed constant equal to unity. Kloppers and Kröger perform a critical comparison of this with the Poppe method, which allows local calculation of the Lewis factor [38]. The comparison shows noticeable differences in performance predictions, with the Poppe method tracking experimental results much more closely. Furthermore, the Poppe method enables outlet dry bulb temperature to be an output of the model, completely necessary for the analysis of a recuperated cooling cycle.

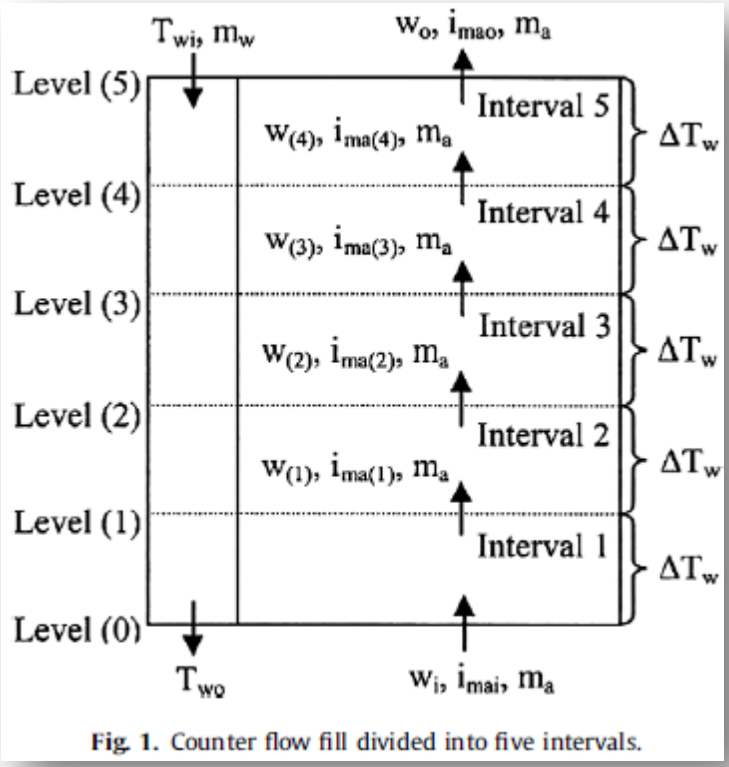

Figure 26. Multiple cells allow more accurate model of the direct contact heat exchange and evaporation process. Image taken from [39].

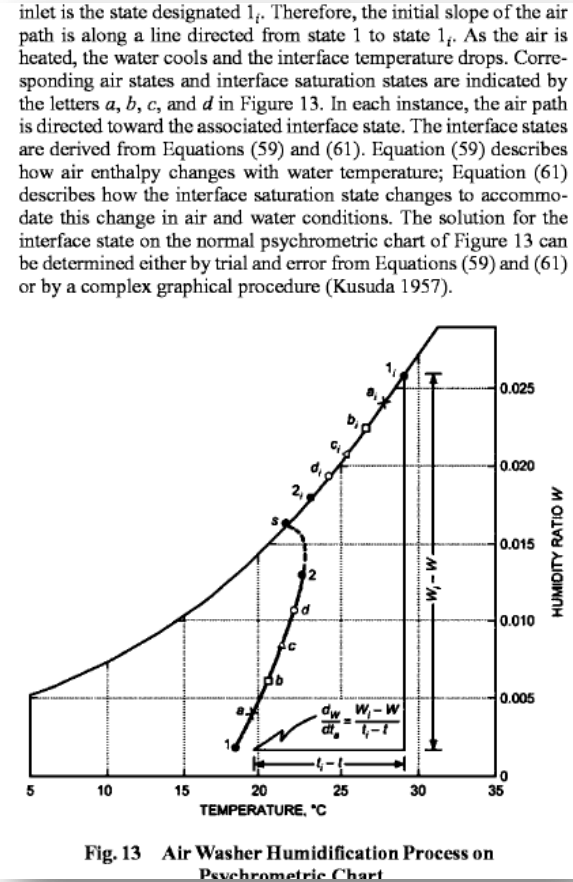

Figure 27. Example multicell calculation of an evaporative process for humidification and heating from literature [37].

3.3 Inlet cooling comparison

Per turbine, the requirement for inlet cooling varies with ambient temperature as shown in Figure 28, which considers a turbine inlet temperature goal of 40 °C maximum to avoid damage and 15 °C for operation at the ISO rating condition and higher electrical output. The values for turbine inlet cooling, $\dot{Q}_{IC}$, are calculated from

$$\dot{Q}_{IC} = \left(\dot{m}c_p\right)_{air}\left(T_{ambient} - T_{goal}\right) \quad \textbf{(17)}$$

where $\left(\dot{m}c_p\right)_{air}$ is …., …. As the first chapter shows, some designs will produce a significant amount of cooling capacity, enough to meet the inlet cooling requirement up to such and such temperature.

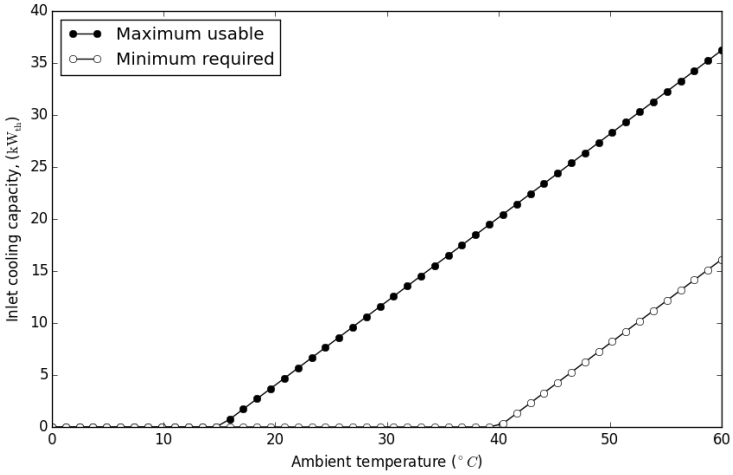

Figure 28. Inlet cooling capacity requirement per turbine.

For this work, the cooling tower models as discussed in the previous section will be integrated with the chiller models from the previous chapter. Over a range of possible psychrometric states, we will calculate the water consumption for spray cooling, and for the same amount of water consumption determine the additional cooling capacity available from the chiller. We will also look at the power and chiller output with the water consumption dialed down to 50%, 20%, and 10% of the level for which 100% of the heat rejection is taken up by latent heat of evaporation and the lowest temperature water is output by the cooling tower.

3.4 Conservative controls for heat rejection

Suppose the system uses a hybrid cooling tower in which the water consumption rate can be dialed down to zero, while the effective temperature returns to ambient. Again the goals for this work will be explained via an example. Using the modelling approach described in the previous section, a case study will be performed of a particular site for which historical weather data are available describing the ambient psychrometric states. These data are available for instance in the form of TMY3 files for Phoenix, AZ from NREL [40]. Figure shows this distribution as a histogram in psychrometric space. Figure 30 shows as a cumulative distribution the projection of the histogram from psychrometric space to each of dry bulb, wet bulb, and dew point temperatures as well as water outlet temperatures for 50% effectiveness for both direct and indirect type cooling towers. In other words, the number of hours per year when the temperature for heat rejection is below a given level varies depending on the type of heat rejection system. Since These results suggest that a system designed for installation in Phoenix, if water is available for consumption, can indeed use the standard value of 29 °C for heat rejection, and could also use an economizer mode for part of the year.

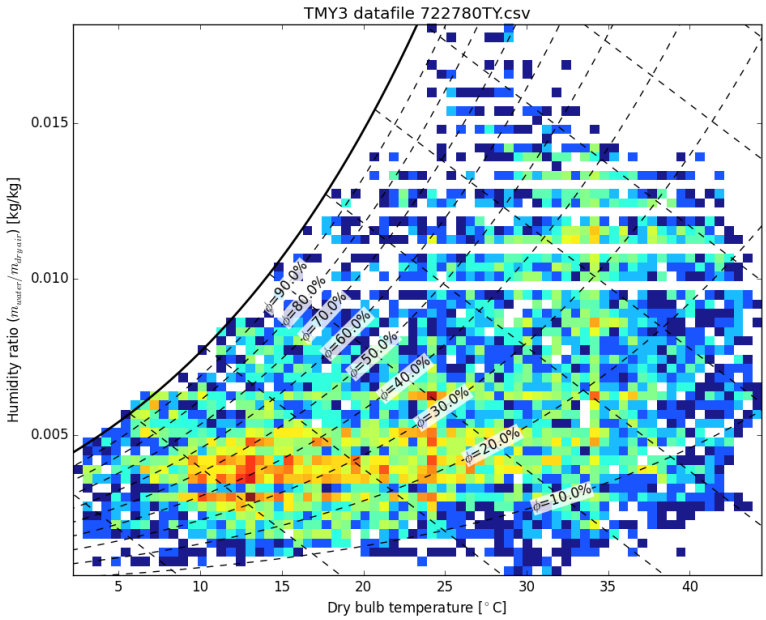

Figure 29. Probability distributions of ambient conditions calculated from TMY3 data for Phoenix [40].

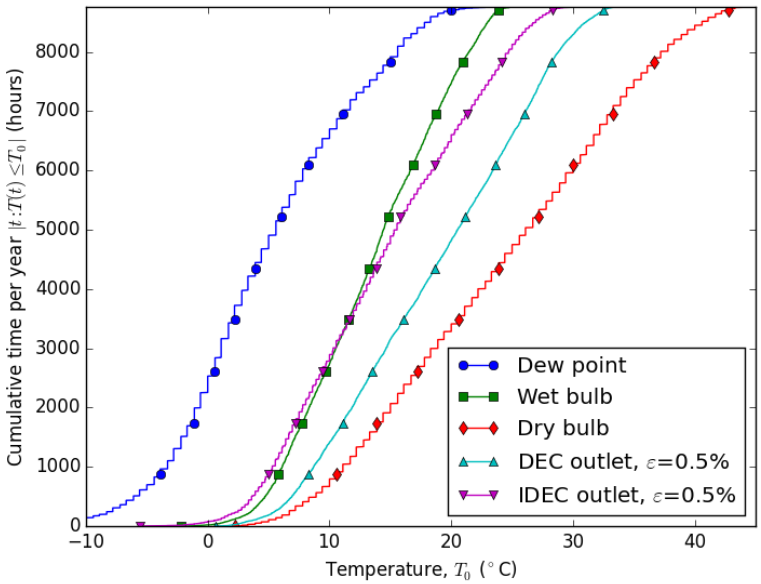

Figure 30. Cumulative probability distributions of some effective temperatures for dry bulb and dew point, including direct evaporative cooler (DEC) and indirect evaporative cooler (IDEC), again calculated from TMY3 data for Phoenix [40].

A control algorithm for water consumption will essentially adjust the effectiveness of the cooling tower and output cooled water between the ambient and effective temperature limit for that tower. Thus the control algorithm would output a water consumption rate as a function of ambient condition (eg. Figure

31), and as a result, its own histogram. Figure 32 shows an example highlighting the features of importance. There may be ambient conditions in which operating the system becomes impossible regardless of water usage, for example because of the crystallization limit for LiBr chillers. For the remaining states, low marginal returns in cooling capacity may make preferable the reallocation of water from time intervals where cooling capacity already meets demand to time intervals where cooling capacity would be below a specified threshold without water use, or when excess cooling can be stored to meet demand at a time of chiller shutdown. Incorporating storage suggests also that a control algorithm design should also utilize conditional probabilities of pairs of ambient conditions separated by a given time delay. This work will encompass a review on existing methods for such a control algorithm design, followed by optimization trials using a variety of constraints and objective functions, then simulation over actual time histories from outside the training data set to demonstrate robustness. There are several computational platforms that may be useful for this work, such as the Scipy optimization routines available freely in Python; the GenOpt tool; or Matlab and Simulink software suite.

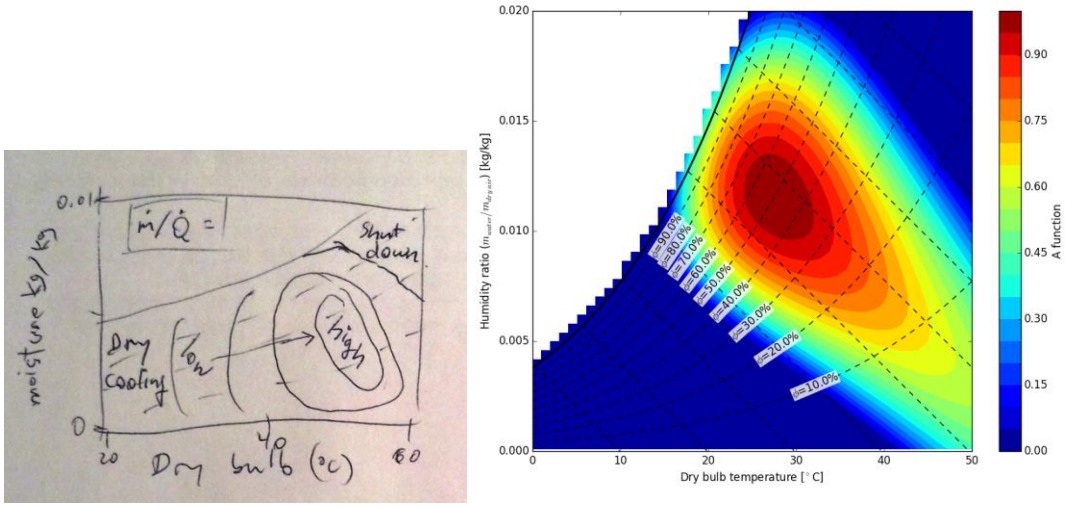

Figure 31. Possible water consumption allocation as a function of ambient condition based on probability, shown as contours of water consumption per unit of heat rejected (kg/kJ) over the psychrometric state space.

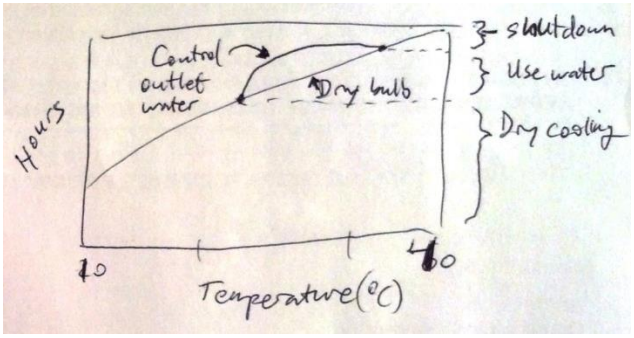

Figure 32. Possible probability distribution for cooled water outlet temperature resulting from control algorithm and simulation with historical data.

Related to the question of how to define an objective function or appropriate constraints for controls optimization is the question of how to value power and other energy services and water as resources to the community. An interesting interplay between these services occurs when the power cycle can also contribute to the water supply via atmospheric moisture capture; pumping water for transport, irrigation, and/or energy storage; and much more practical desalination. To analyze this problem requires a broad techno-economic and sustainable development perspective, which is encouraged as a future work outside the scope of this dissertation.

3.5 Summary and next steps

The potential to optimize chiller cooling capacity by allowing for some water consumption in the heat rejection process is clear, and some analysis of the optimal heat rejection system design and control should be carried out to determine the best possible performance from the waste heat driven cooling system.

4 Cooling in high ambient temperatures

4.1 Introduction

In this chapter we outline focus on the effect of high ambient temperatures and analyze the changes in standard cooling cycle performance, then consider several options for cooling cycles that operate robustly under those conditions. In this we also include ejector cooling cycles and hybrid combinations such as ejector-assisted absorption cooling. Additionally, we consider an absorption cycle design approach based on matching the heat vs temperature profile of a Brayton turbine.

First, let us mention miscellaneous thoughts. Bovea et al. [41] reported a comparative life cycle analysis of commonly used refrigerants in commercial refrigerant systems. Interestingly, Elbel and Hrnjak [21] point out that there have been instances of unsupported claims regarding ejector cycle performance, as well as some paradoxical results in the literature on the performance subject to high ambient temperature of compression cycles with an ejector pump used for energy recovery in the expansion element.

4.1.1 Some data about ambient temperatures and rating conditions

In many climates, temperatures are already hot, and they are getting hotter. According to both the IPCC [42] and the industry handbook, "The evidence is unequivocal that the climate system is warming globally" [20, p. 14.13]. More people need cooling where it is hot. Figure 33 shows an excerpt with some relevant data.

The evidence is unequivocal that the climate system is warming globally (IPCC 2007). The most frequently observed effects relate to increases in average, and to some degree, extreme temperatures.

This is partly illustrated by the results of an analysis of design conditions conducted as part of calculating the values for the 2009 edition of this chapter (Thevenard 2009). For 1274 observing sites worldwide with suitably complete data from 1977 to 2006, selected design conditions were compared between the period 1977-1986 and 1997-2006. The results, averaged over all locations, are as follows:

- The 99.6% annual dry-bulb temperature increased 1.52 K
- The 0.4% annual dry-bulb increased 0.79 K
- Annual dew point increased by 0.55 K
- Heating degree-days (base 18.3°C) decreased by 237°C-days
- Cooling degree-days (base 10°C) increased by 136°C-days

Figure 33. Some data about ambient temperatures, from [20].

Table 5 shows some standards and guidelines that suggest nominal conditions to be used for performance ratings tests. Additionally, the Low-GWP Alternative Refrigerants Evaluation Program has specified a number of test conditions for compressor testing [43]. Note however that those specify

internal temperatures; for example, a “high” discharge dew point temperature of 57.2 °C is mentioned to correspond to a “high” ambient temperature of 46.1 °C.

Table 5. Applicable test standards for condenser external temperatures

Equipment	Standard	Description
Turbine [3], air inlet	ISO 2314 [44]	Dry bulb 15 °C
Absorption chiller [6], condenser water	JIS B 8622	Inlet 29.4 °C Outlet 36.4 °C
Absorption chiller [45], condenser water	ARI 560-2000	Inlet 29.4 °C Outlet 38.5 °C
Vapor compressor test [43, p. 106]	“ISO T3”	Indoor DB = 29 °C, WB = 19 °C, Outdoor DB = 46 °C
Vapor compressor test [43, p. 106]	“Optional test condition”	Indoor DB = 29 °C, WB = 19 °C, Outdoor DB = 52 °C
Room air conditioner [46]	ISO5151-T1	Moderate climate Air cooled units: Outdoor DB = 35 °C, WB = 24 °C Water cooled units: Inlet 30 °C, Outlet 35 °C
Room A/C [46]	ISO5151-T2	Cool climate Air cooled units: Outdoor DB = 27 °C, WB = 19 °C Water cooled units: Inlet 22 °C, Outlet 27 °C
Room A/C [46]	ISO5151-T3	Hot climate Air cooled units: Outdoor DB = 46 °C, WB = 24 °C Water cooled units: Inlet 30 °C, Outlet 35 °C

4.2 Future work: matching heat input demand to heat source

When ambient temperature is high, one way to improve performance is to remove every possible source of exergy destruction by challenging assumptions about the conventional design approach. As indicated in sections 2.2.2 and 2.3.2, matching the shape of the application heat input to the shape of the heat source in heat vs temperature coordinates allows the most heat and exergy to be initially recovered. Thus there is a case to be made for a chiller design approach that attempts to reduce the exergy destruction in transferring heat to the chiller. This section presents four methods for this: first, configurations using multiple chillers that draw from the heat source at different temperatures; second, custom chiller cycle having multiple components accepting heat input at different temperatures; third, ejector cycles with mixtures that increase temperature glide; and fourth, trans-critical ejector cycles.

4.2.1 Multiple chillers

An observation was made that for most of the cooling cycles, the shape of the temperature vs heat input curve for the internal fluid stream accepting the heat is flat, i.e., at or near a single temperature level. Therefore, the heat input to multiple chillers can be viewed as a set of rectangular blocks on the heat exchange diagram. By neglecting exergy destruction due to heat transfer at the ambient heat rejection and cooling delivery interfaces, and assuming that chillers operate a fixed fraction of Carnot efficiency at all conditions, an analytic result for optimal temperatures may be obtained: the optimal operating temperatures form a geometric series. Initial results using this approach are presented in Figure 34. A new version of this simple model in EES will include a method for describing realistic heat

exchanger performance. Regarding a path for implementing the results of this work, it is noted that single-effect and double-effect LiBr chillers can be found in the product brochure literature that operate near the optimal temperatures for a pair of these technologies, but that crystallization limits need to be studied for the double-effect system to guarantee stable operation. To visualize the series configuration case, Figure 34 shows a schematic and a heat transfer diagram with availability on the vertical axis to show as area the exergy content of heat inputs driving the two chillers.

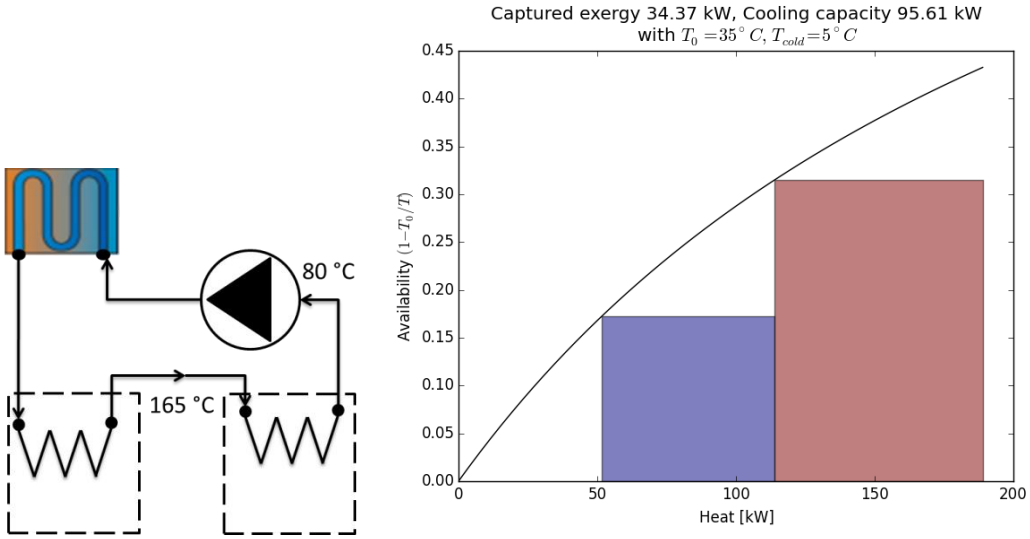

Figure 34. Multiple chillers drawing heat from heat source in series: conceptual schematic (left, not actual temperatures) and rescaled heat exchange diagram (right). Box areas show exergy supplied to the high effect chiller (red) and low effect (blue).

For the cases of more chillers, Figure 35 shows some of the trends for total exergy captured, and cooling capacity resulting from the assumption that chillers operate at 30% of the Carnot efficiency. These show that, based on the aforementioned assumptions, increasing the number of chillers increases the maximum exergy recovery and cooling that can be achieved, with dimishing returns. A further work on this could be to relate the cost of each chiller to its size and operating temperature; however, as the result is not specific to a certain technology, the utility of cost results would be questionable.

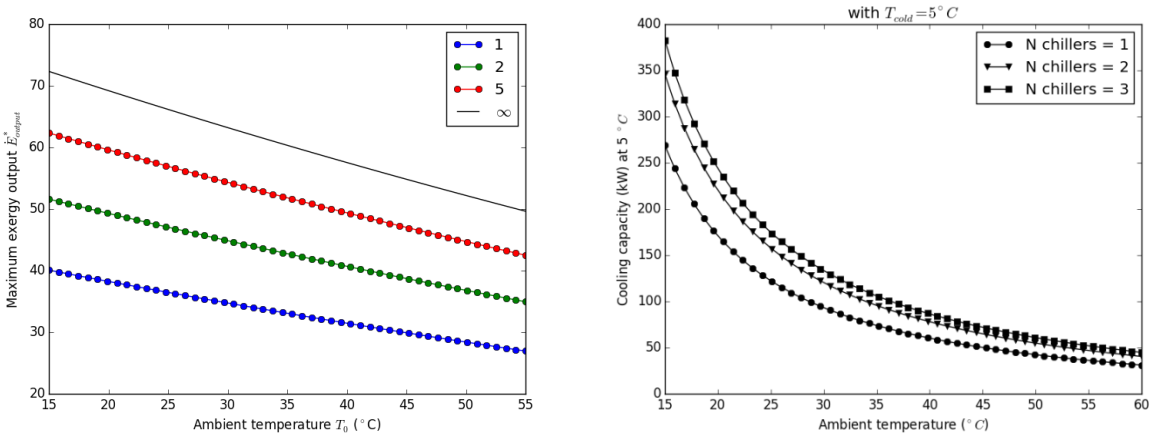

Figure 35. Multiple chillers: naïve model trends for optimal configurations.

For cases of one through five chillers, the optimal captured heat profile is shown Figure 36 by overlaying the exergy block plots.

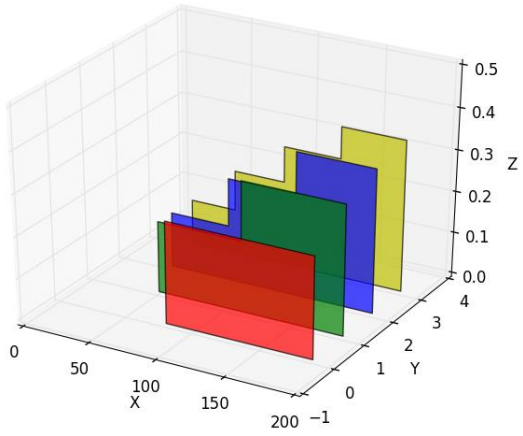

Figure 36. Multiple chillers: optimal temperatures for each case from one through five chillers.

4.2.2 Custom absorption chiller design

For the custom chiller cycle design case, one pathway for capturing more exergy is to arrange a series of generators at increasing pressures in a single chiller design. (A comparable concept in the literature for power cycles is to introduce taps for feed heater stream pressure from multiple pressure stages in a turbine. Bejan shows how to optimize those pressure levels [47, p. 380].) This would look similar to a multiple effect chiller, but could have external heat input to each generator, and potentially therefore generate more refrigerant vapor at each pressure, as shown in Figure 37. Obviously, it would also have a lower COP than a high effect absorption unit, but it would be able to capture more of the heat input because of placement of the pinch point for heat recovery, as discussed for example in section 2.3.2.

Lithium bromide and ammonia water are reasonable choices for starting the analysis, but there are other options. For reference, Alefeld describes data needed for choosing fluid pairs [48], and Karamangil et al. demonstrate working fluid comparisons using a numerical model [49].

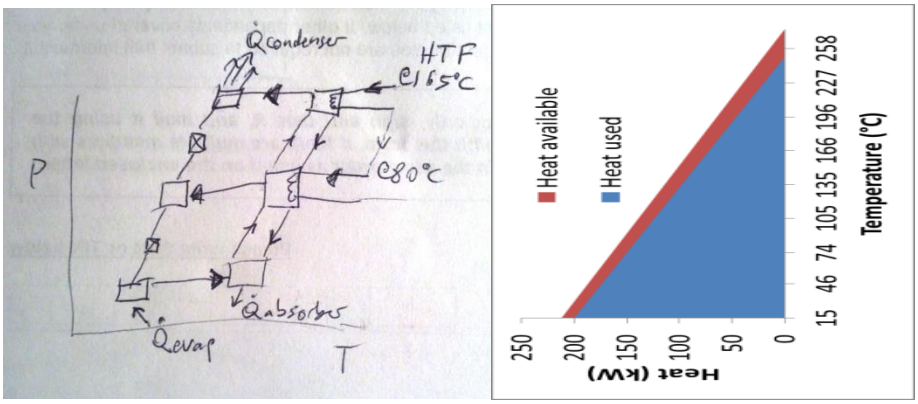

Figure 37. Conceptual schematic (left) for a custom chiller design intended to match the heat source profile. Increasing the number of levels could allow the grand composite curve for heat input to approach an ideal case (right). [TODO: re-draw figure on right]

4.2.3 Ejector cycles with mixtures

Mixtures may exhibit temperature glide through constant pressure, constant composition boiling curves. Typically, saturated liquid temperature is lower than saturated vapor temperature. This means the T-h curve slopes upward, allowing a closer match to the heat source curve as described above. A study on fluid selection and mixture optimization has not been found in the literature for the particular waste heat stream under consideration. To gain experience useful for this work, analysis was performed for an arbitrary mixture. Other refrigerants and refrigerant mixtures for use in ejector cycles are discussed in the literature, and future work is to repeat the analysis methodically for a variety of refrigerants.

The example model is an ejector cycle using for both motive and refrigerant flows a mixture of ethanol-water of concentration 40% ethanol by mass. Figure 38 shows some of the state points for an arbitrary set of inputs for internal pressure levels. The model produces reasonable solutions, but the cooling cycle doesn't work well, having a low COP, and very low lift capability. So-called "wet" vapor saturation curve results in low performance. Some temperature glide is achieved but not much: 11 °C. For this effort, we created an open-source demonstration of how to access NIST's REFPROP database, which includes additional mixtures, from the popular solver, EES. This allows us to extend the study to a number of other mixtures. (In this analysis, it is assumed that the concentration is uniform.)

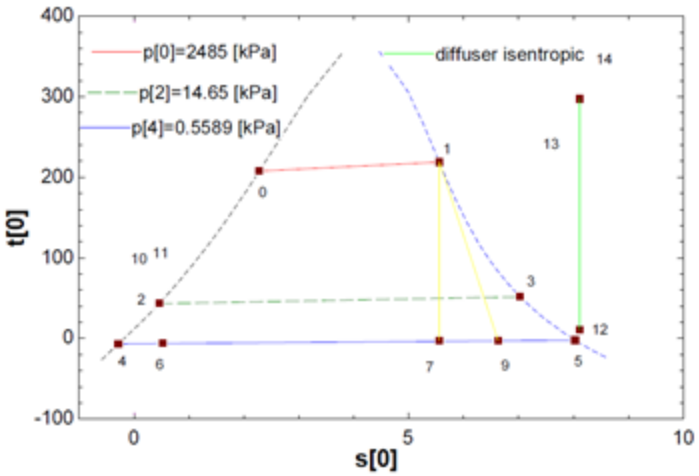

Figure 38. Some state points from numerical model of ejector cycle with a mixture of 40% by mass ethanol in water.

4.2.4 Fluid selection for trans-critical ejector cycle

A trans-critical generator would pass above instead of through the vapor dome. This often results in a better fit to a straight line in the T-h plane, as needed to match the heat source profile. Therefore a search for fluids with a critical temperature around 150 °C to 200 °C should be conducted and ejector cycle performance computed. This may be aided by guides to ejector cycle design and fluid databases such as REFPROP.

4.3 Future work: modified cycles at high ambient temperatures

Nonconventional cycles (with low historical usage) have been developed and analyzed that may have performance advantages at high ambient. In [50], Mehr et al. modelled the absorption (GAX) ejector hybrid shown in Figure 39, found to be competitive with the double effect ammonia-water cycle in terms of heat input temperature, but with much higher allowable heat rejection temperature (up to 70 °C). Additional concepts for absorption cycles and ejector cycles respectively may be found in dissertations by Liao [51] and Pridisawas [52].

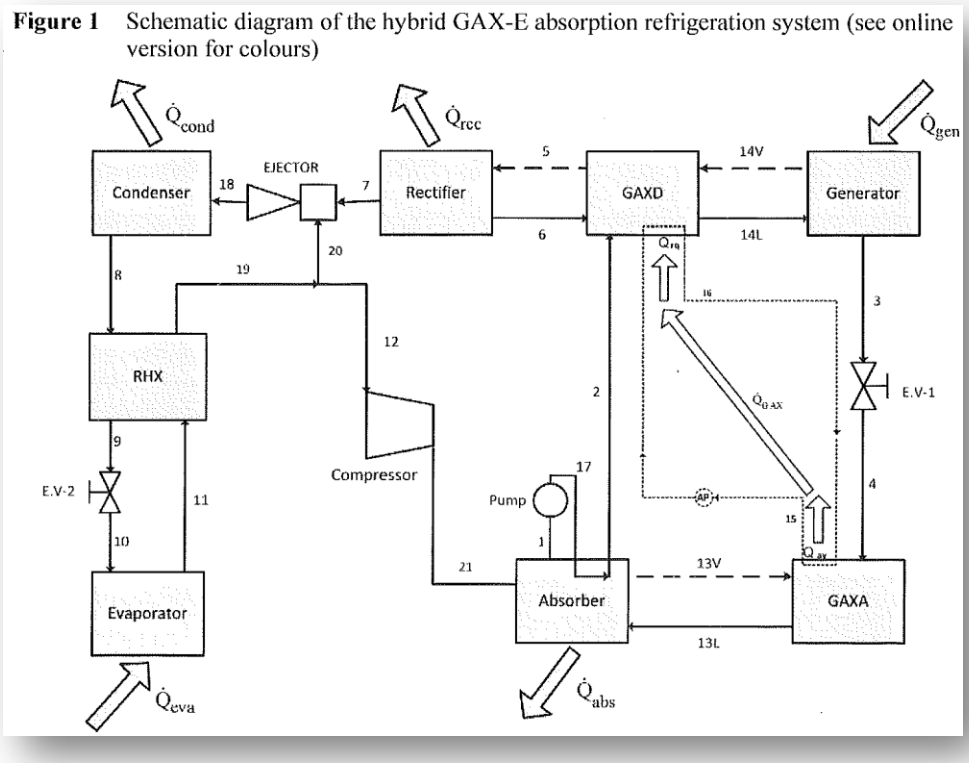

Figure 39. A cycle modified to recover energy from refrigerant expansion, from [50].

4.4 Miscellaneous methods

A variety of concepts should also be examined via literature review and modeling for their potential to improve performance of heat recovery and cooling cycle.

- The manufacturing technology for 3D printed heat exchangers allows geometry optimization to reduce pressure drop and increase effectiveness. Incorporating heat exchangers with high overall heat transfer coefficients would allow reduced pinch point temperature differences and improve performance as shown in Chapter 2. A challenge is the material compatibility between materials that can be printed and refrigerants; for example, absorption cycle fluids can be quite corrosive.
- Geometry-free optimization of thermal cycles has been proposed but not found in the literature. A one-page description is available describing the concept, which is inspired both by constructal law for flow system optimization and genetic-algorithm-driven material removal tools for structural optimization, but an example has yet to be created which will demonstrate whether the idea is practical and what is required for an implementation. This concept could be used to develop an approach for thermal cycle ideation.
- Two-fluid ejector cycles have the potential to allow somewhat independent selection of the motive fluid and refrigerant in order to increase the efficiency of the power half cycle and cooling half cycle. However, a general approach to modelling ejector pumps for immiscible fluid pairs remains to be found in the literature.

- Direct contacting absorption heat recovery has been proposed for recovering enthalpy from water vapor in flue gas in a manner similar to a wet scrubbing but with calcium nitrate added to reduce the equilibrium vapor pressure and therefore increase the moisture and heat recovered [53]. Note that calcium-based sorbents have previously been used for desulfurization and studied for carbon-capture applications, as well [54]. For indirect condensing heat exchangers, best practices have been suggested including use of a water-spray-bed [55].

4.5 Summary and next steps

Several non-conventional designs have been proposed and should be analyzed. High ambient temperatures should be applied in the analysis. Using computational tools and cycles composed of the basic components modeled in the previous chapters, numerical models can be created for the analyses.

5 Summary

In this document, a number of methods for design and analysis of waste-heat driven cooling systems have been presented, focused on an application to a novel renewable energy platform in development, as discussed in Section 1.3. A summary of completed work, Chapter 2, shows the value of detailed design analysis in aiding the technology selection decisions for chillers given the unique constraints of the heat source. Next, Chapter 3 illustrates the potential value of considering a variety of heat rejection techniques, and the future work on this will enable decisions for heat rejection system selection and control design based on quantitative results from simulation. Finally, Chapter 4 presents the reasons to re-consider cooling system design choices and impose high ambient temperatures for the analysis. Future work outlined therein will identify which options have the greatest potential to increase cooling capacity and will create the quantitative framework for design optimization by analysis. These works will proceed following the schedule outlined in Section 1.2.

6 Acknowledgements

The author would like to thank for their fruitful discussions, encouragement, and support: the committee members; the members of the lab group; Jon Sherbeck, Valeriy Khaldarov, Shivani A Saptarishy, Kunal N Parikh, Paul A Strong, Ce Ji, Weixiao Li, and all the “Cooler Devils” team members in the Max Tech and Beyond AY2013-2014 competition as well as the administrators and mentors at Lawrence Berkeley National Lab; Herb Hayden, Memo Romero, Mark Miner, Tyler Beeney, Chao-Han Lin, Bradley Stone, and everyone at Southwest Solar Technology, LLC, as well as collaborators on solar applications including Madeline Tyson and the SCORE Algae team; and Rob Taylor and Ali Shirazi at UNSW. Also would like to thank Marcus Myers, Colin Laisure-Pool and the other members of ASHRAE Central Arizona Chapter, and Karl Edelhoff of ASU Facilities for helping me learn about building energy; and the many students from courses that I have assisted to teach, who have all taught me. Appreciation should not be overlooked for additional help from correspondents including Gershon Grossmann, Ursula Eicker, Daniel Mugnier, Uli Jakob, and chiller manufacturers. Finally, many thanks are due to Pinchas Doran and AORA Solar Ltd for keeping solar-powered microturbines running and for funding the work on combined systems, and to President Michael Crow and LightWorks for establishing research collaborations. Additional thanks are offered to the Mechanical Engineering department for the opportunities to study, teach, and research here.

7 Works Cited

[1] AORA Solar Ltd, "Product," AORA Solar Ltd, [Online]. Available: http://aora-solar.com/product/. [Accessed 28 Apr 2015].

[2] C. Dorgan, S. Leight and C. Dorgan, Application guide for absorption cooling/refrigeration using recovered heat, Atlanta: American Society of Heating, Refrigerating, and Air-Conditioning Engineers, Inc, 1995.

[3] Turbec Spa, "T100 microturbine system D14127-03 Technical description Ver 3," Turbec Spa, Corporeno, Italy, 29 Dec 2009.

[4] C. D. Moné, D. S. Chau and P. E. Phelan, "Economic feasibility of combined heat and power and absorption refrigeration with commercially available gas turbines," *Energy Conversion and Management,* vol. 41, pp. 1559-1573, 2001.

[5] Y. Gupta, L. Metchop, A. Frantzis and P. Phelan, "Comparative analysis of thermally activated, environmentally friendly cooling systems," *Energy Conversion and Management,* vol. 49, no. 5, pp. 1091-1097, 2008.

[6] Broad Air Conditioning, *Broad X non-electric chiller: model selection and design manual,* Changsha, China, 2008.

[7] P. Bombarda, C. M. Invernizzi and C. Pietra, "Heat recovery from Diesel engines: A thermodynamic comparison between Kalina and ORC cycles," *Applied Thermal Engineering,* vol. 30, no. 2-3, pp. 212-219, 2009. http://dx.doi.org/10.1016/j.applthermaleng.2009.08.006.

[8] R. Sirwan, M. Alghoul, K. Sopian, Y. Ali and J. Abdulateef, "Evaluation of adding flash tank to solar combined ejector-absorption refrigeration system," *Solar Energy,* vol. 91, pp. 283-296, 2013. http://dx.doi.org/10.1016/j.solener.2013.01.018.

[9] U. G. SD, "PERSONA / OPERARIO," GrabCad, 21 08 2015. [Online]. Available: https://grabcad.com/library/persona-operario-1. [Accessed 12 10 2015].

[10] S. Reiter, Industrial and Commercial Heat Recovery Systems, New York: Van Nostrand Reinhold Company, 1983.

[11] H. H. Kruse, "Current Status and Future Potential of Nonazeotropic Mixed Refrigerants," in *Heat Pumps: Prospects in Heat Pump Technology & Marketing*, Chelsea, Michigan, Lewis Publishers, Inc, 1987, pp. 173-194.

[12] K. E. Herold, R. Radermacher and S. A. Klein, Absorption Chillers and Heat Pumps, Boca Raton: CRC Press, 1996.

[13] J. L. Boyen, Thermal Energy Recovery, New York: John Wiley & Sons, Inc, 1980.

[14] M. Olszewski and M. E. J. Gunn, "Recovery of Industrial Waste Heat: Waste Heat Recovery Techniques," in *Utilization of Reject Heat*, New York and Basel, Marcel Dekker, Inc, 1980, pp. 73-94.

[15] M. Nishio, K. Shiroko and T. Umeda, "A Thermodynamic Approach to Steam-Power System Design," *I&EC Process Design & Development,* vol. 19, pp. 306-312, 1980.

[16] R. F. Boehm, Design Analysis of Thermal Systems, New York: John Wiley & Sons, Inc, 1987.

[17] A. Bejan, Entropy generation through heat and fluid flow, New York: John Wiley & Sons, Inc, 1982.

[18] R. W. Serth, Process Heat Transfer: Principles and Applications, Burlington, MA: Elsevier Ltd, 2007.

[19] Y. A. Çengel, Heat and Mass Transfer, 3rd edition, New York: McGraw-Hill, 2007.

[20] ASHRAE, "Climatic Design Information," in *Handbook: Fundamentals*, Atlanta, ASHRAE, Inc, 2009, p. 14.*.

[21] S. Elbel and P. Hrnjak, "Ejector Refrigeration: An Overview of Historical and Present Developments with an Emphasis on Air Conditioning Applications," in *International Refrigeration and Air Conditioning Conference*, Urbana, Illinois, 2008.

[22] K. P. Tyagi and K. N. Murty, "Ejector-compression systems for cooling: utilising low grade waste heat," *Heat Recovery Syst,* vol. 5, pp. 545-50, 1985. http://dx.doi.org/10.1016/0198-7593(85)90222-X.

[23] I. Eames, S. Aphornratana and D.-W. Sun, "The jet-pump cycle--A low cost refrigerator option powered by waste heat," *Heat Recovery Systems and CHP,* vol. 15, no. 8, pp. 711-721, 1995.

[24] S. Varga, A. C. Oliveira and B. Diaconu, "Analysis of a solar-assisted ejector cooling system for air conditioning," *International Journal of Low-Carbon Technologies,* vol. 4, no. 1, pp. 2-8, 2009. doi:10.1093/ijlct/ctn001.

[25] S. Varga, A. C. Oliveira and B. Diaconu, "Numerical assessment of steam ejector efficiencies using CFD," *International Journal of Refrigeration,* vol. 32, no. 6, pp. 1203-1211, 2009. http://dx.doi.org/10.1016/j.ijrefrig.2009.01.007.

[26] G. Untea, A. Dobrovicescu, L. Grosu and E. Mladin, "Energy and Exergy Analysis of an Ejector Refrigeration System," *UPB Sci. Bull. Ser. D Mech. Eng,* vol. 75, no. 4, pp. 111-126, 2013.

http://www.scientificbulletin.upb.ro/rev_docs_arhiva/fullb14_527495.pdf.

[27] M. Dennis and K. Garzoli, "Use of variable geometry," *International journal of refrigeration,* vol. 34, pp. 1626-1632, 2011. http://dx.doi.org/10.1016/j.ijrefrig.2010.08.006.

[28] O. Ayadi, M. Aprile and M. Motta, "Solar cooling systems utilizing concentrating solar collectors - An overview," in *Energy Procedia 30*, San Francisco, 2012.

[29] ASHRAE, "Chap 13: Steam-jet refrigeration," in *Equipment handbook*, Atlanta, ASHRAE, 1979, pp. 13.1-13.6.

[30] E. D. Rogdakis and G. K. Alexis, "Design and parametric investigation of an ejector in an air-conditioning system," *Applied Thermal Engineering,* vol. 20, pp. 213-226, 2000. http://dx.doi.org/10.1016/S1359-4311(99)00013-7.

[31] ASHRAE, Handbook: HVAC Systems and Equipment, Atlanta: ASHRAE, 2012.

[32] ASHRAE, "Psychrometrics," in *Handbook -- Fundamentals*, Atlanta, American Society of Heating, Refrigeration, and Air-conditioning Engineers, Inc, 2012, p. Chapter 1.

[33] ASHRAE, "Cooling Towers," in *Handbook -- HVAC Systems and Equipment*, Atlanta, American Society of Heating, Refrigeration, and Air-conditioning Engineers, Inc, 2012, p. Chapter 40.

[34] N. H. DesChamps, "Workshop on Modern Evaporative Cooling Technologies: Advanced Evaporative Cooling Technologies -- Commercial," 10 July 2007. [Online]. Available: http://www.swenergy.org/events/evaporative/presentations/Nick_DesChamps_Munters-DesChamps.pdf. [Accessed May 2014].

[35] E. Kozubal and S. Slayzak, "Coolerado 5 Ton RTU Performance: Western Cooling Challenge Results," National Renewable Energy Laboratory, Golden, Colorado, 2010.

[36] DesChamps Heat Exchangers and Energy Recovery Systems, *Heat pipe heat exchanger (product catalog),* Natural Bridge Station, Virginia: Munters - Des Champs Laboratories Incorporated, 1998.

[37] ASHRAE, "Mass Transfer," in *Handbook: Fundamentals*, Atlanta, ASHRAE, Inc., 2013, pp. 6.1-6.14.

[38] J. C. Kloppers and D. G. Kröger, "Cooling Tower Performance Evaluation: Merkel, Poppe, and e-NTU Methods of Analysis," *Journal of Engineering for Gas Turbines and Power,* vol. 127, pp. 1-7, 2005. http://dx.doi.org/10.1115/1.1787504.

[39] E. Rezaei, S. Shafiei and A. Abdollahnezhad, "Reducing water consumption of an industrial plant cooling unit using hybrid cooling tower," *Energy Conversion and Management,* vol. 51, pp. 311-319, 2010. http://dx.doi.org/10.1016/j.enconman.2009.09.027.

[40] National Renewable Energy Laboratory (NREL), "National Solar Radiation Data Base," 19 Jan 2015. [Online]. Available: http://rredc.nrel.gov/solar/old_data/nsrdb/1991-2005/tmy3/. [Accessed 26 Mar 2014].

[41] M. D. Bovea, R. Cabello and D. Querol, "Comparative Life Cycle Assessment of Commonly Used Refrigerants in Commercial Refrigeration Systems," *Internation Journal of Life Cycle Analysis,* vol. 12, no. 5, pp. 299-307, 2007.

[42] Intergovernmental Panel on Climate Change (IPCC), "Fifth Assessment Report (AR5)," Cambridge University Press, Cambridge, United Kingdom and New York, NY, USA, 2013-2014.

[43] Air-Conditioning, Heat, and Refrigeration Institute, "AHRI Low-GWP Alternative Refrigerants Evaluation Program (Low-GWP AREP)," AHRI, Arlington, VA, 2015. http://www.ahrinet.org/App_Content/ahri/files/RESEARCH/Participants_Handbook2015-04-17.pdf.

[44] International Standards Organization, *ISO 2314, Gas-turbines -- Acceptance tests,* 1989.

[45] York, *YIA Single-Effect Absorption Chillers Steam And Hot Water Chillers,* Johnson Controls.

[46] EnergyConsult, *Comparison of International MEPS: Room Air Conditioners,* Victoria, Australia: The Australian Greenhouse Office: National Appliance & Equipment Energy Efficiency Program, 2005. http://www.energyrating.gov.au/wp-content/uploads/Energy_Rating_Documents/Library/Cooling/Air_Conditioners/200503-acmeps-internat.pdf.

[47] A. Bejan, Advanced Engineering Thermodynamics, New York: John Wiley & Sons, 2006, p. 635.

[48] G. Alefeld, "What needs to be known about fluid pairs to determine heat ratios of absorber heat pumps and heat transformers," in *HEAT PUMPS: Prospects in Heat Pump Technology and Marketing*, Chelsea, Michigan, Lewis Publishers, 1987, pp. 375-387.

[49] M. Karamangil, S. Coskun, O. Kaynakli and N. Yamankaradeniz, "A simulation study of performance evaluation of single-stage absorption refrigeration system using conventional working fluids and alternatives," *Renewable and Sustainable Energy Reviews,* vol. 14, pp. 1969-1978, 2010. http://dx.doi.org/10.1016/j.rser.2010.04.008.

[50] A. Mehr, S. Mahmoudi, M. Yari and A. Soroureddin, "A novel hybrid GAX-ejector refrigeration cycle with an air-cooled absorber," *International Journal of Exergy,* vol. 13, no. 4, pp. 447-471, 2013.

[51] X. Liao, "the development of an air-cooled absorption chiller concept and its integration in chp systems," Department of Mechanical Engineering, University of Maryland, College Park, 2004.

[52] W. Pridasawas, Solar-Driven Refrigeration Systems with Focus on the Ejector Cycle: a Doctoral

Thesis, Stockholm: Royal Institute of Technology, KTH, 2006.

[53] S. K. Hong, S. Park, C. Ko and K. Choi, *Poster: Experimental Study on Characteristics of Heat Recovery System Using Absorption Solution,* San Diego: ASME Power & Energy Conference, 2015.

[54] H. Zhang, H. Tong, S. Wang, Y. Zhuo, C. Chen and X. Xu, "Simultaneous Removal of SO2 and NO from Flue Gas with Calcium-Based Sorbent at Low Temperature," *Industrial & Engingeering Chemistry Research,* vol. 45, no. 18, p. 6099–6103, 2006.

[55] S. Hong, S.-i. Park, S.-Y. Jeon and K.-S. Lee, "Experimental study on heat transfer characteristics of water-spray-bed heat exchanger," *Journal of Mechanical Science and Technology,* vol. 29, no. 5, pp. 2243-2247, 2015. http://dx.doi.org/10.1007/s12206-015-0445-y.